Transport signatures of fractional quantum Hall binding transitions

Transport signatures of fractional quantum Hall binding transitions

Christian Spånslätt,[1,2,3,*] Ady Stern,[4] and Alexander D. Mirlin[2,3]

[1]*Department of Microtechnology and Nanoscience (MC2), Chalmers University of Technology, S-412 96 Göteborg, Sweden*
[2]*Institute for Quantum Materials and Technologies, Karlsruhe Institute of Technology, 76021 Karlsruhe, Germany*
[3]*Institut für Theorie der Kondensierten Materie, Karlsruhe Institute of Technology, 76128 Karlsruhe, Germany*
[4]*Department of Condensed Matter Physics, Weizmann Institute of Science, Rehovot 7610001, Israel*

(Received 11 February 2023; revised 22 May 2023; accepted 23 May 2023; published 5 June 2023)

Certain fractional quantum Hall edges have been predicted to undergo quantum phase transitions which reduce the number of edge channels and at the same time bind electrons together. However, detailed studies of experimental signatures of such a "binding transition" remain lacking. Here, we propose quantum transport signatures with focus on the edge at filling $\nu = 9/5$. We demonstrate theoretically that in the regime of nonequilibrated edge transport, the bound and unbound edge phases have distinct conductance and noise characteristics. We also show that for a quantum point contact in the strong back-scattering (SBS) regime, the bound phase produces a minimum Fano factor $F_{\mathrm{SBS}} = 3$ corresponding to three-electron tunneling, whereas single-electron tunneling is strongly suppressed at low energies. Together with recent experimental developments, our results will be useful for detecting binding transitions in the fractional quantum Hall regime.

DOI: 10.1103/PhysRevB.107.245405

I. INTRODUCTION

Edges of fractional quantum Hall (FQH) states [1,2] are outstanding platforms for strongly correlated electron physics. A FQH edge realizes the so-called chiral Luttinger liquid [3–8], which is a set of one-dimensional conducting channels inheriting topological properties of the FQH bulk state. The chiral Luttinger liquid has been successfully used to investigate a wide variety of fundamental quantum phenomena, e.g., topological quantization, charge fractionalization [9–11], anyonic statistics [12,13], topological quantum computation [14], or quantum phase transitions [15–17].

A particularly striking FQH edge quantum phase transition, called the binding transition, was proposed by Kao *et al.* [18], based on earlier work by Haldane [19]. In the binding transition, pairs of oppositely propagating edge channels localize due to an edge instability triggered by interchannel particle tunneling and strong interactions. The remaining edge channels may then carry excitations with electrical charges different from those of the original edge; charges that can be viewed as bound composites of electrons.

Binding transitions are possible only for so-called T-unstable FQH states, defined as those states permitting charge-neutral and bosonic quasiparticle excitations lacking topological content in their correlation function [17,19]. On the edge, the creation and annihilation operators of such excitations describe charge tunneling between edge channels, and appear in the edge Hamiltonian without breaking any symmetries. Physically, it is only T-unstable edges that permit pairs of oppositely propagating channels to localize. Equivalently, T-unstable edges have low-energy charge-neutral fixed points with an equal number of neutral modes (we use the terms "mode" and "channel" interchangeably in this work) propagating in each direction [17]. Importantly, the binding transition does not alter the topological order of the FQH bulk state and is therefore a pure edge transition, amenable for detection in edge experiments.

The simplest example of the binding transition was predicted for the edge at filling factor $\nu = 9/5$ (see Fig. 1). In the free, or unbound, phase, the $9/5$ edge hosts three channels, which after the binding transition are reduced to a single channel. Most remarkably, in this so-called bound phase, single electron excitations become short ranged and do not participate in the low-energy edge transport. By contrast, excitations with charges $3e$ remain long ranged and do contribute to the transport [18]. Despite such a striking reorganization of the edge structure, the prospects of experimentally observing a binding transition remain to large extent unexplored.

In this paper, we address this issue by proposing several experimental signatures of the binding transition. Our work is motivated by novel developments for probing FQH edges with quantum transport (a recent overview is given in Ref. [20]). More specifically, a growing body of experiments have demonstrated the existence of a wide range of different edge transport regimes. These range from complete charge and heat equilibration of the edge channels [21–23], to intermediate regimes with full charge but no heat equilibration [24–28], to the extreme limit of nonequilibrated charge transport [29,30]. To detect a binding transition, access to nonequilibrated

*christian.spanslatt@chalmers.se

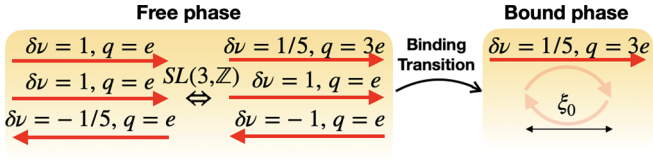

FIG. 1. The FQH binding transition at filling $\nu = 9/5$. The free edge phase comprises two downstream propagating channels (right-pointing arrows), both with filling factor discontinuities $\delta\nu = 1$ and charge $q = e$ (here, the charge q is the minimum charge that can tunnel across vacuum into the channel). There is also one upstream channel filling factor discontinuity $\delta\nu = -1/5$ and charge $q = e$ (left-pointing arrow). This structure is equivalent [after a $SL(3, \mathbf{Z})$ basis change] to a Laughlin edge state with $\delta\nu = 1/5$ composed of charge $q = 3e$ composite particles, plus two counterpropagating channels with $\delta\nu = \pm 1$ and $q = e$. The binding transition is the phenomenon where interchannel interactions and tunneling cause the counterpropagating channels to localize (with characteristic low-temperature length scale ξ_0). In the bound phase, only the single composite channel remains.

transport regimes is of particular interest, since in these regimes, the charge and heat conductances do not necessarily reflect the bulk topological order. Instead, these quantities can reveal the total number of edge channels and the charges they carry, quantities that both change across the binding transition. In addition, recent experiments [31,32], have demonstrated robust, engineered FQH edges formed between regions with different bulk fillings. For example, an "artificial" 9/5 edge can be synthesized by proximitizing regions with fillings $\nu = 2$ and $1/5$. Such structures, which might allow experimental control over Landau level spin polarizations and thereby tunneling rates between edge channels, facilitate the detection of binding transitions.

As a key result, we find that the two edge phases have different charge and heat conductance characteristics (see Table I). With decreasing level of equilibration (i.e., with decreasing temperature T and/or system size L), the free phase conductances monotonously increase from the values for equilibrated transport, which defines regime $\mathcal{III}$, to saturation at the nonequilibrated values, defining regime $\mathcal{II}$. By contrast, the bound phase is characterized by the existence of a localized regime, regime $\mathcal{I}$, with similar characteristics as regime $\mathcal{III}$. A transition between regimes $\mathcal{I}$ and $\mathcal{II}$ is possible for strong interactions and give rise to the unusual situation of increasing conductances with increasing temperature. Such an observation is a striking hallmark of the existence of edge localization. Complementing the conductances, we further argue that a current biased edge segment produces shot noise, S, when the charge transport is equilibrated but the heat transport is not. This feature occurs only for strong interactions, associated with the bound phase, in regime $\mathcal{II}$.

We also demonstrate that in a quantum point contact (QPC) device in the strong back-scattering (SBS) regime, the bound phase yields a minimum shot noise Fano factor $F_{\mathrm{SBS}} = 3$ corresponding to three-electron tunneling. No single electron tunneling is possible at low energies. This result stands in stark contrast to the free phase, where strong back-scattering favours single electron tunneling, i.e., $F_{\mathrm{SBS}} = 1$. By the same token, in the weak back-scattering (WBS) regime, the most

TABLE I. Transport characteristics for the $\nu = 9/5$ edge. For the free and bound edge phases, values for the two-terminal electrical (G) and heat ($G^{\mathcal{Q}}$) conductances, the shot noise S of a current biased edge segment, and QPC Fano factors for strong, F_{SBS}, and weak F_{WBS} back scattering regimes are given. There are three relevant transport regimes. Regime $\mathcal{I}$: regime of localization, $\mathcal{II}$: no localization but vanishing equilibration, and $\mathcal{III}$ full edge equilibration. The emergence of regime $\mathcal{I}$ for the bound phase is a fundamental feature of the binding transition. The quantized $G^{\mathcal{Q}}$ values in regime $\mathcal{II}$ are given under the assumption of vanishing interference in edge-contact plasmon scattering: $L \gg L_T \sim T^{-1}$. The noise in regime $\mathcal{II}$ is given under the condition (77) of efficient charge equilibration and poor thermal equilibration. This condition holds for strong interactions which is only the case in the bound phase.

Regimes	Transport charact.	Free	Bound
$\mathcal{I}$	$G/(e^2/h)$	–	9/5
	$G^{\mathcal{Q}}/(\kappa T)$	–	1
	S	–	0
$\mathcal{II}$	$G/(e^2/h)$	11/5	11/5
	$G^{\mathcal{Q}}/(\kappa T)$	3	3
	S [10^{-29}A^2/(nA Hz)]	$\simeq 0$	0.25–0.7
$\mathcal{III}$	$G/(e^2/h)$	9/5	9/5
	$G^{\mathcal{Q}}/(\kappa T)$	1	1
	S	$\simeq 0$	0
QPC Fano factors	F_{SBS}	1	3
	F_{WBS}	1/5	3/5

relevant (in the renormalization group, RG, sense) quasiparticle tunneling yields in the bound phase $F_{\mathrm{WBS}} = 3/5$, in contrast to the free phase value $F_{\mathrm{WBS}} = 1/5$. Altogether, our set of derived transport signatures present several possibilities for experimentally detecting a FQH binding transition.

The remainder of this paper is organized as follows. In Sec. II, we review the basics of the FQH edge theory and the binding transition. We also perform a renormalization group (RG) treatment of the transition. In the main part of this paper, Sec. III, we derive several transport signatures of the bound phase and contrast them to those of the free phase. In Sec. IV, we discuss possible experimental setups to detect the proposed signatures. We summarize in Sec. V and also provide an outlook towards future studies.

Throughout this paper, we generally use units $e = \hbar = k_{\mathrm{B}} = 1$, but we restore important units for transport observables.

II. THE CHIRAL LUTTINGER LIQUID AND THE BINDING TRANSITION

For completeness, we review here key aspects of the chiral Luttinger theory and the FQH binding transition, closely following Refs. [16–18].

A. Chiral Luttinger liquid

At low energies, an Abelian FQH edge is well described by the chiral Luttinger liquid (χ_{LL}) model, specified by the pair $(K, \mathbf{t})$ [5]. Here, K is an $n \times n$ integer valued symmetric matrix, and the charge vector $\mathbf{t}$ is an n-dimensional vector of

integers. The generic n-channel action reads

$$S_{\chi_{LL}} = -\frac{1}{4\pi}\int dtdx[\partial_t \boldsymbol{\phi}^T K \partial_x \boldsymbol{\phi} + \partial_x \boldsymbol{\phi}^T V \partial_x \boldsymbol{\phi}], \quad (1)$$

where $\boldsymbol{\phi} = (\phi_1, \ldots, \phi_n)$ is a set of bosonic fields obeying the commutation relations

$$[\phi_i(x), \phi_j(y)] = i\pi K^{-1}_{ij}\mathrm{sgn}(x-y). \quad (2)$$

The symmetric matrix V in (1) parametrizes the channel velocities, V_{ii}, and mutual, short-range Coulomb interactions, $V_{i\neq j}$. Generally, V contains $n(n+1)/2$, independent, nonuniversal parameters, determined by microscopic details in the edge electrostatic confinement.

The electrical charge enters the theory in the charge densities

$$\rho_i \equiv t_i \frac{\partial_x \phi_i}{2\pi}, \quad (3)$$

which obey

$$[\rho_i(x), \rho_j(y)] = \frac{i}{2\pi} t_i^2 K^{-1}_{ij} \partial_x \delta(x-y). \quad (4)$$

Several quantities determined by the bulk topological order appear in the edge theory. The filling factor ν is given as

$$\nu = \mathbf{t}^T K^{-1} \mathbf{t}, \quad (5)$$

and the "thermal quantum number" as

$$\nu_Q \equiv \mathrm{Tr}(\eta) = n_d - n_u. \quad (6)$$

Here, η is the signature matrix corresponding to K, so that ν_Q equals the difference in the number of positive and negative eigenvalues of K (i.e., $\eta_{ij} = \pm 1\delta_{ij}$). In turn, this is equivalent to the number of "downstream" n_d and "upstream" n_u propagating channels (with respect to the chirality direction set by the magnetic field) respectively [33,34]. For the present theory of Abelian states, $\nu_Q \in \mathbb{Z}$, while for non-Abelian states, other values of ν_Q are possible. For example, Majorana edge channels allow half-integer values $\nu_Q \in \mathbb{Z}/2$ [22]. As described below in Sec. III, ν_Q is closely connected to the edge heat transport characteristics.

Quasiparticles (including the special case of the electron) created or destroyed at position (t, x) on the edge are described by vertex operators

$$\mathcal{T}_{\mathbf{l}}(t,x) = \frac{e^{i\mathbf{l}\cdot\boldsymbol{\phi}(t,x)}}{(2\pi a)^{m/2}}, \quad (7)$$

where m is the number of involved bosons. A vertex operator is uniquely determined by specifying an integer valued vector $\mathbf{l}$ which describes how many of each quasiparticle species that are created or destroyed. The associated exchange statistics angle $\Theta_{\mathbf{l}}$ and electric charge $Q_{\mathbf{l}}$ of a vertex operator are given by

$$\Theta_{\mathbf{l}} = \pi \mathbf{l}^T K^{-1} \mathbf{l} \mod 2\pi, \quad (8)$$

$$Q_{\mathbf{l}} = \mathbf{t}^T K^{-1} \mathbf{l}. \quad (9)$$

With the use of vertex operators, tunneling of particles between edge channels is included in the theory by adding to (1) the term

$$S_{\mathrm{T}} = \int dtdx\, \xi(x) \mathcal{T}_{\mathbf{l}}(t,x) + \mathrm{H.c}, \quad (10)$$

where $\xi(x)$ is the local tunneling strength at spatial location x. As discussed below in Eqs. (28)–(30), the function $\xi(x)$ determines the type of tunneling between the edge channels.

To compute various observables in the theory, correlation functions involving $\mathcal{T}_{\mathbf{l}}(t,x)$ are needed. These are most easily obtained by diagonalizing $S_{\chi_{LL}}$ which is done by first taking K to its signature matrix η by a (nonunique) matrix M_1

$$M_1^T K M_1 = \eta. \quad (11)$$

Second, a matrix M_2 (also not unique) is sought which diagonalizes V into $\tilde{V}$ but at the same time preserves η:

$$\eta = M_2^T M_1^T K M_1 M_2, \quad (12)$$

$$\tilde{V} = M_2^T M_1^T V M_1 M_2. \quad (13)$$

In the diagonal basis, the action (1) becomes

$$S_{\chi_{LL}} = -\frac{1}{4\pi}\int dtdx[\partial_t \tilde{\boldsymbol{\phi}}^T \eta \partial_x \tilde{\boldsymbol{\phi}} + \partial_x \tilde{\boldsymbol{\phi}}^T \tilde{V} \partial_x \tilde{\boldsymbol{\phi}}] \quad (14)$$

and the theory is now expressible in transformed quantities as

$$\tilde{\boldsymbol{\phi}} = M^{-1}\boldsymbol{\phi}, \quad (15a)$$

$$\tilde{\mathbf{t}} = M^T \mathbf{t}, \quad (15b)$$

$$\tilde{\mathbf{l}} = M^T \mathbf{l}, \quad (15c)$$

with $M \equiv M_1 M_2$. The free, "diagonal," bosons $\tilde{\phi}_i$ and their densities

$$\tilde{\rho}_i \equiv \tilde{t}_i \frac{\partial_x \tilde{\phi}_i}{2\pi}, \quad (16)$$

obey

$$[\tilde{\phi}_i(x), \tilde{\phi}_j(y)] = i\pi \eta_{ij}\mathrm{sgn}(x-y), \quad (17)$$

$$[\tilde{\rho}_i(x), \tilde{\rho}_j(y)] = \frac{i}{2\pi}\tilde{t}_i^2 \eta_{ij}\partial_x \delta(x-y). \quad (18)$$

Note that all topological properties (5), (6), (8), and (9) are independent of the choice of basis. The total charge density is also preserved:

$$\sum_i \rho_i = \sum_i \tilde{\rho}_i. \quad (19)$$

In the diagonal basis, the action is quadratic and correlation functions of vertex operators follow from the identity

$$\langle e^{i\tilde{\phi}_i(t,x)} e^{-i\tilde{\phi}_i(0,0)}\rangle = e^{\langle \tilde{\phi}_i(t,x)\tilde{\phi}_i(0,0) - \langle \tilde{\phi}_i^2(0,0)\rangle} = \frac{a}{a + x - i\eta_i \tilde{v}_i t}, \quad (20)$$

upon use of the zero temperature correlation function

$$\langle \tilde{\phi}_i(t,x)\tilde{\phi}_i(0,0)\rangle - \langle \tilde{\phi}_i^2(0,0)\rangle = -\ln\left[\frac{a + x - i\eta_i \tilde{v}_i t}{a}\right]. \quad (21)$$

In Eqs. (20) and (21), $\eta_i \equiv \eta_{ii}$ and $\tilde{v}_i \equiv \tilde{V}_{ii}$ is the chirality and the speed of mode $\tilde{\phi}_i$, respectively. We also introduced a short distance (ultraviolet, UV) cutoff a on the order of the

characteristic magnetic length. At finite temperature T, the correlation function (21) changes to

$$\langle\tilde{\phi}_i(t,x)\tilde{\phi}_i(0,0)-\langle\tilde{\phi}_i^2(0,0)\rangle = -\ln\left[\frac{\sin\left(\frac{\pi T}{\tilde{v}_i}(a+x-i\eta_i\tilde{v}_i t)\right)}{\pi aT/\tilde{v}_i}\right]. \quad (22)$$

By combining the single mode correlation (20) with the transformation rules (15), the (zero T) correlation function of $\mathcal{T}_{\mathbf{l}}(t,x)$ is obtained as

$$\langle\mathcal{T}_{\mathbf{l}}(t,x)\mathcal{T}_{\mathbf{l}}^\dagger(0,0)\rangle \sim \langle e^{i\mathbf{l}\cdot\boldsymbol{\phi}(t,x)}e^{-i\mathbf{l}\cdot\boldsymbol{\phi}(0,0)}\rangle = \langle e^{i\tilde{\mathbf{l}}\cdot\tilde{\boldsymbol{\phi}}(t,x)}e^{-i\tilde{\mathbf{l}}\cdot\tilde{\boldsymbol{\phi}}(0,0)}\rangle = \prod_i\left(\frac{a}{a+x-i\eta_i\tilde{v}_i t}\right)^{(\tilde{\mathbf{l}}_i)^2}. \quad (23)$$

The long-time behavior

$$\langle\mathcal{T}_{\mathbf{l}}(t,0)\mathcal{T}_{\mathbf{l}}^\dagger(0,0)\rangle \propto \frac{1}{t^{\kappa(\mathbf{l})}}\frac{1}{|t|^{2\Delta(\mathbf{l})-\kappa(\mathbf{l})}}, \quad (24)$$

where

$$\Delta(\mathbf{l}) \equiv \frac{1}{2}\tilde{\mathbf{l}}^T\tilde{\mathbf{l}} = \frac{1}{2}\mathbf{l}^T MM^T\mathbf{l}, \quad (25)$$

$$\kappa(\mathbf{l}) \equiv \tilde{\mathbf{l}}^T\eta^{-1}\tilde{\mathbf{l}} = \mathbf{l}^T K^{-1}\mathbf{l} \quad (26)$$

defines the scaling dimension and the topological part of the correlation function, respectively. The generic scaling dimension (25) is nonuniversal, as it depends not only on the topological matrix K but also on the components of V. An exception occurs for so-called maximally chiral edges, in which all channels propagate in the same direction, i.e., either n_d or n_u equals zero. Then, the scaling dimensions of tunneling operators are fully specified by K alone.

Importantly, $\kappa(\mathbf{l})$ and $\Delta(\mathbf{l})$ obey the following inequality [17]:

$$|\kappa(\mathbf{l})| \leqslant 2\Delta(\mathbf{l}), \quad (27)$$

with equality for vanishing interactions (diagonal V). For maximally chiral edges, Eq. (27) becomes an equality independently of interactions.

We now consider tunnel coupled edge channels, so that the total action $S = S_{\chi LL} + S_{\mathrm{T}}$. Depending on the nature of the tunneling events, S_{T} becomes an RG relevant perturbation when

$$3-2\Delta(\mathbf{l})>0, \quad \langle\xi(x)\xi^*(y)\rangle = D\delta(x-y), \quad (28)$$

$$1-\Delta(\mathbf{l})>0, \quad \xi(x)=\Gamma_0\delta(x), \quad (29)$$

$$2-\Delta(\mathbf{l})>0, \quad \xi(x)=\Gamma_0, \quad (30)$$

corresponding to Gaussian random (characterized by the strength D), single point, and uniform tunneling, respectively. In this paper, we mainly focus on the common situation of random interchannel tunneling due to quenched (static) edge disorder. (Point tunneling as realized in a QPC is considered in Sec. III D). To guarantee the relevancy of $\mathcal{T}_{\mathbf{l}}$, Eq. (28) implies that $\Delta(\mathbf{l}) < 3/2$. By virtue of Eq. (27), this implies further

$$|\kappa(\mathbf{l})| \leqslant 2\Delta(\mathbf{l}) < 3. \quad (31)$$

In turn, any tunneling operator must be bosonic, which by use of Eq. (8) implies that $\kappa(\mathbf{l})$ must be an even integer. This fact, combined with Eq. (31), implies that

$$\kappa(\mathbf{l}) = -2, 0, 2, \quad (32)$$

for random, relevant tunneling operators. As we shall see next, when a very particular class of such tunneling operators exist and are relevant, a FQH edge will undergo a binding transition.

B. Review of the binding transition

The binding transition is only possible for so-called T-unstable edges. These are defined as those edges permitting a special kind of quasiparticles (which we parametrize for convenience by $\mathbf{m}$ rather than $\mathbf{l}$), satisfying the two constraints [18,19]

$$\mathbf{m}^T K^{-1}\mathbf{m} = 0, \quad (33)$$

$$\mathbf{t}^T K^{-1}\mathbf{m} = 0. \quad (34)$$

A nonzero string $\mathbf{m}$ obeying these constraints is called a null vector, and Eqs. (33) and (34) are called the null conditions. They are invariant under basis transformations.

The possibility to satisfy the null conditions can be traced to the existence of counterpropagating neutral modes in the charge-neutral basis [17]. Physically, the null operators create charge-neutral and bosonic particles without any topological part in their correlation function (24). Then, and only then, is it possible for pairs of edge channels to undergo localization. We may view this feature as the edge structure containing a nontopological part which can be removed by the nontopological disorder and interactions.

We can readily check that no null vectors exist for edges (those with nonzero Hall conductance) with one or two channels, i.e., for $n = 1, 2$. For $n = 1$, we have $\mathbf{m} = m$, $\mathbf{t} = t$, and K^{-1} is an odd integer. Equations (33) and (34) then read

$$K^{-1}m^2 = 0, \quad (35)$$

$$tK^{-1}m = 0, \quad (36)$$

which is only trivially satisfied by $m = 0$.

For $n = 2$, we may choose without loss of generality

$$K = \begin{pmatrix} 1/\delta\nu_1 & 0 \\ 0 & 1/\delta\nu_2. \end{pmatrix}, \quad \mathbf{m}^T = (m_1, m_2), \quad \mathbf{t}^T = (1,1). \quad (37)$$

Here, $\delta\nu_{1,2}$ (the eigenvalues of K^{-1}) are known as "filling factor discontinuities" and specify jumps in the Hall fluid density close to the edge. For example, the $\nu = 2/3$ edge is specified by $\delta\nu_1 = 1$ and $\delta\nu_2 = -1/3$ [15]. The null conditions (33) and (34) now read

$$m_1^2\delta\nu_1 + m_2^2\delta\nu_2 = 0, \quad (38)$$

$$m_1\delta\nu_1 + m_2\delta\nu_2 = 0. \quad (39)$$

These equations have only the trivial $m_1 = m_2 = 0$ solution, under the condition $\delta\nu_1 \neq \delta\nu_2$, which must be satisfied for the $n = 2$ chiral Luttinger liquid [5]. With the present formalism,

we can however readily see that for a standard, spinless Luttinger liquid, i.e., for $\delta\nu_1 = -\delta\nu_2 = 1$, all charge conserving ($m_1 = m_2$) operators satisfy (38) and (39) and may cause instabilities localizing the edge channels [35,36] (see also Ref. [37] for a recent discussion).

For $n = 3$, there exists several T-unstable FQH states. Specifically, we focus as follows on the state at filling $\nu = 9/5$. The corresponding edge theory is defined by

$$K = \begin{pmatrix} 1 & 0 & 0 \\ 0 & 1 & 0 \\ 0 & 0 & -5 \end{pmatrix}, \quad \mathbf{t}^T = (1, 1, 1). \tag{40}$$

Using the null conditions (33) and (34), it can readily be checked that

$$\mathbf{m}_1^T = (-1, 2, 5), \quad \mathbf{m}_2^T = (2, -1, 5), \tag{41}$$

are the two possible null vectors (changing an overall sign does not count as a new null vector). We denote the corresponding null operators by

$$\mathcal{V}_{\mathbf{m}_j}(t, x) \sim e^{i\mathbf{m}_j \cdot \boldsymbol{\phi}(t,x)}, \quad j = 1 \text{ and } 2. \tag{42}$$

With the scaling dimension formula (25), one can check that in the absence of interactions, i.e., when V is diagonal in basis (40), the scaling dimensions of these operators are $\Delta(\mathbf{m}_1) = \Delta(\mathbf{m}_2) = 5$, whereas interactions reduce these values.

The binding transition becomes possible when at least one of the null operators (42) is RG relevant [18], i.e., $\Delta(\mathbf{m}_j) < 3/2$, according to Eq. (28). This requires sufficiently strong edge interactions. As follows, we now assume, without loss of generality [18], that $\mathcal{V}_{\mathbf{m}_1}$ is a relevant operator and ignore all effects from $\mathcal{V}_{\mathbf{m}_2}$.

To understand the binding transition, it is very useful to perform a basis transformation with a matrix $W \in SL(3, \mathbb{Z})$. With the appropriate choice of W (the exact details of W are not important, but its existence follows from the existence of null vectors), we can equally represent the 9/5 edge as

$$K' = \begin{pmatrix} 5 & 0 & 0 \\ 0 & 1 & 0 \\ 0 & 0 & -1 \end{pmatrix}, \quad \mathbf{t}'^{\mathbf{T}} = (3, 1, 1). \tag{43}$$

In this basis, the null vectors read

$$\mathbf{m}_1'^{\mathbf{T}} = (0, 1, 1), \quad \mathbf{m}_2'^{\mathbf{T}} = (15, -2, 7). \tag{44}$$

We focus only on the null vector $\mathbf{m}_1'$ and its associated null operator $\mathcal{V}_{\mathbf{m}_1'}$. Note that this operator only couples two of the three modes. The absence of interactions in the basis (43), happens when the scaling dimension of $\mathcal{V}_{\mathbf{m}_1'}$ is $\Delta(\mathbf{m}_1') = 1$. We emphasize that the effects on the system by addition of $\mathcal{V}_{\mathbf{m}_1'}$ and $\mathcal{V}_{\mathbf{m}_2'}$ are equivalent. Indeed, a simple basis change can be made such that instead $\mathbf{m}_2'^{\mathbf{T}} = (0, 1, 1)$.

Equation (43) suggests that the 9/5 edge can be viewed as two counterpropagating channels with filling factor discontinuities ± 1 carrying unit charge, and one downstream channel with filling factor discontinuity 1/5 carrying particles with charge $3e$ (see Fig. 1). These composite particles can be thought of "Cooper triplons": bound states of three electrons. Unlike conventional Cooper pairs, however, the composite particles here are fermionic and therefore cannot condense.

The binding transition is the manifestation of localization of the two equal and counterpropagating channels due to interactions and disorder [35,36]. After localization, only one channel remains. In some sense, this can be thought of as an "inverted edge reconstruction," where nontopological pairs of channels vanish rather than appear. On length scales much larger than a characteristic localization length (to be discussed in more detail below in Sec. II C), the edge structure is then effectively given as

$$K = (5), \quad \mathbf{t}^T = (3), \tag{45}$$

which is nothing but a $\nu = 1/5$ Laughlin state made out of charge $3e$ composites. The peculiarity of the binding transition is that when two counterpropagating but otherwise equal channels localize, the remaining channel carries a changed charge as to preserve the topological quantum numbers from the bulk. This picture clarifies also why $n = 3$ is the minimum number of edge channels required for a binding transition.

From Eqs. (43) and (44), we see that excitations (7) with vectors

$$\mathbf{l}'^{\mathbf{T}} = (0, q, q), \quad q \in \mathbb{Z}, \tag{46}$$

will become localized on the edge, i.e., those $\mathbf{l}'$ satisfying

$$\mathbf{l}'^{\mathbf{T}} K'^{-1} \mathbf{m}_1' = 0. \tag{47}$$

Due to the transformation rules (15), the condition (47) holds in any basis. In contrast, an excitation on the form

$$\mathbf{l}'^{\mathbf{T}} = (p, 0, 0), \quad p \in \mathbb{Z} \tag{48}$$

will propagate freely along the edge. In more technical terms, in the original three-dimensional vector-space of excitations, only excitations in the one-dimensional subspace of vectors $\mathbf{l}'$ satisfying

$$\mathbf{l}'^{\mathbf{T}} \mathbf{K}'^{-\mathbf{1}} \mathbf{m}_1' = 0 \text{ and } \mathbf{l}' \text{ not proportional to } \mathbf{m}_1' \tag{49}$$

will propagate freely on the bound edge. From Eqs. (8) and (9), we see that the statistics and the charge of the propagating excitations (48) are

$$\Theta_{\mathbf{l}'} = \pi \frac{p^2}{5}, \tag{50}$$

$$Q_{\mathbf{l}'} = \frac{3p}{5}. \tag{51}$$

Since only $p = 5N$, with N an odd integer produces quantum numbers consistent with the electron, it follows that only electron excitations in bunches of 3 can propagate. In contrast, single electron excitations become localized on the edge. The consequence of this effect is explored in more detail in Sec. III D. In passing, we note that for bosonic FQH states, N must be even to preserve Bose statistics. This implies that binding transitions for such states always generate even multiples of bound composites.

The goal of this paper can now be formulated as investigating the transport properties for the edge in the two different edge phases. To this end, we next perform an RG analysis to find the phase diagram of the edge.

C. Scaling analysis of the binding transition

Our simple scaling analysis of the binding transition follows the approach in Refs. [35,36,38]. Throughout this section, we assume that $\mathcal{V}_{\mathbf{m}'_1}$ [see Eq. (42)] is more relevant than $\mathcal{V}_{\mathbf{m}'_2}$ and analyze here only the influence of $\mathcal{V}_{\mathbf{m}'_1}$. The opposite situation can be treated in a perfectly analogous manner.

For convenience, we next redefine the disorder strength in Eq. (28) so that it becomes dimensionless (see Appendix A). We thus set

$$D \to D \times \frac{a^{3-m}}{v^2}. \tag{52}$$

Here, m is the number of bosonic fields involved in the null operator $\mathcal{V}_{\mathbf{m}_1}$, i.e., $m = 3$, and v is a characteristic velocity (i.e., some combination of the v_i; the exact details are not important here). The first-order renormalization equation for D then reads [35]

$$\frac{\partial D}{\partial \ln(L/a)} = (3 - 2\Delta_0)D, \tag{53}$$

where Δ_0 is the initial scaling dimension of $\mathcal{V}_{\mathbf{m}'_1}$, L is the system size, and a is the UV length cutoff (e.g., the magnetic length). The physical meaning of $D(L)$ is the inverse dimensionless conductance at the scale L. In what follows, we ignore effects of renormalization of Δ_0, as they only weakly affect the renormalization of disorder [36,38] and are thus nonessential for our analysis. Hence, in what follows, we take

$$\Delta \approx \Delta_0 \tag{54}$$

during the RG flow. It follows from Eq. (53) that

$$D(L) = D_0 \left(\frac{L}{a}\right)^{3-2\Delta_0}, \tag{55}$$

where $D_0 \equiv D(L = a)$ is the bare (nonrenormalized) disorder strength, assumed to be weak: $D_0 \ll 1$.

We now study the consequences of Eqs. (53) and (55) in the two regions $\Delta_0 > 3/2$ and $\Delta_0 < 3/2$.

1. $\Delta_0 > 3/2$

For $\Delta_0 > 3/2$, $D(L)$ decreases upon renormalization towards lower energies (i.e., with increasing L), so that strong localization (which requires $D(L) \gtrsim 1$) does not take place at any length scale. Consequently, the edge is in the free phase, described by Eq. (40) or (43). Tunneling between the edge modes remains weak at all energies. This tunneling exchanges charge and heat among the edge channels which causes equilibration. We denote the characteristic length scales for charge and heat equilibration as ℓ_C respectively ℓ_Q. They are both nonuniversal as they depend on microscopic details such as disorder, interactions, and the temperature. Generically, a FQH edge is characterized by two such length scales for each pair of edge modes [39,40]. However, only tunneling between counterpropagating channels can partition charge and energy flows and influence transport coefficients. The quantities ℓ_C and ℓ_Q should then be understood as the dominating ones in the full set.

The temperature scalings of ℓ_C and ℓ_Q are expected to be the same [38]. In the case of equilibration between nonequivalent counterpropagating modes (such as $+1$ and $-1/3$ in the $\nu = 2/3$ edge), strong interactions can cause parametrically different prefactors [24]. We do not see an obvious reason for this in the present case of equilibration between $+1$ and -1 modes. Also, our main interest is in the temperature scaling. We thus treat the equilibration length scales on the same footing by setting

$$\ell_C \sim \ell_Q \sim \ell_{eq}, \tag{56}$$

and ℓ_{eq} is to be understood as meaning both ℓ_C and ℓ_Q.

To find the temperature scaling of ℓ_{eq}, we first note that with weakening disorder, the RG flow is cut at the thermal length

$$L_T \sim vT^{-1}. \tag{57}$$

At this scale, the disorder has, according to Eq. (55), the strength

$$D(L_T) = D_0 \left(\frac{L_T}{a}\right)^{3-2\Delta_0} \propto T^{2\Delta_0 - 3}. \tag{58}$$

At larger length scales $L > L_T$, $D(L)$ scales linearly in L (which is a conventional dependence of classical resistance of a wire with length L):

$$D(L) \sim \frac{L}{L_T} D(L_T) \sim \frac{L}{L_T} D_0 \left(\frac{L_T}{a}\right)^{3-2\Delta_0}, \tag{59}$$

where we used Eq. (58) in the final step. The equilibration length is defined as

$$D(\ell_{eq}) \sim 1, \tag{60}$$

which yields, according to Eq. (59),

$$\ell_{eq} \sim D_0^{-1} a \left(\frac{L_T}{a}\right)^{2\Delta_0 - 2} \propto T^{2-2\Delta_0}. \tag{61}$$

Note that $2 - 2\Delta_0 < 0$ in the regime $\Delta_0 > 3/2$, so that ℓ_{eq} and thus both ℓ_C and ℓ_Q increase with decreasing temperature [16,24].

We can then identify two possible regimes in the free phase.

(1) At lowest temperatures, such that $L \ll \ell_C, \ell_Q \sim T^{2-2\Delta_0}$, the three modes in the free phase are neither charge nor heat equilibrated. The temperature scaling exponent depends nonuniversally on interchannel interactions and velocities. We call this regime $\mathcal{II}$: the regime of absent localization and poor equilibration.

(2) At higher temperatures: $\ell_C, \ell_Q \ll L$ the three edge modes become fully equilibrated, which we denote as regime $\mathcal{III}$. Here, the edge is expected to be governed by hydrodynamic behavior due to interchannel scattering [41].

We depict regimes $\mathcal{II} - \mathcal{III}$ for the free phase in Fig. 2(c).

2. $\Delta_0 < 3/2$

For $\Delta_0 < 3/2$, Eq. (55) shows that $D(L)$ grows during renormalization (i.e., with increasing L). The characteristic length scale ξ_0 at which the disorder becomes strong,

$$D(\xi_0) \sim 1, \tag{62}$$

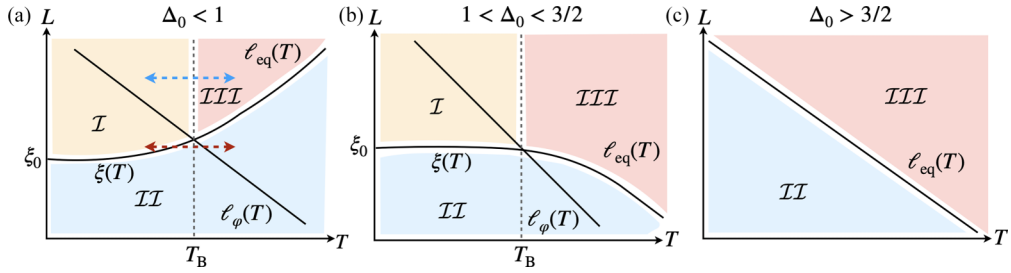

FIG. 2. Schematic log-log "phase diagrams" of transport regimes in the parameter plane spanned by the temperature T and the length scale L at which the system is observed. The point ξ_0 on the L axis in (a) and (b) is the zero-temperature localization length (63). A full line starting from this point is the temperature-dependent localization length $\xi(T)$; after crossing the line $T = T_B$ it becomes the equilibration length $\ell_{eq}(T) \propto T^{2-2\Delta_0}$, see Eq. (64), with Δ_0 being the scaling dimension of the null operator. Further, $\ell_\varphi \propto 1/T$ is the electron-electron scattering length (66). The vertical dashed line is the characteristic temperature scale T_B for onset of localization, which is defined by the condition $\ell_\varphi(T_B) = \ell_{eq}(T_B)$ and is given by Eq. (67). In (a) and (b), localization occurs in regime $\mathcal{I}$ (yellow region), whereas regimes $\mathcal{II}$ (blue region) and $\mathcal{III}$ (red region) correspond to nonequilibrated and equilibrated transport, respectively. In (c), localization is absent. The blue and red, dashed lines depict crossovers $\mathcal{I} \to \mathcal{III}$ and $\mathcal{I} \to \mathcal{II}$, respectively. Note that the latter crossover is only possible for $\Delta_0 < 1$.

yields the zero-temperature localization length ξ_0 [35,36]. Substituting Eq. (55) into the condition (62), one finds

$$\xi_0 \sim a D_0^{-1/(3-2\Delta_0)}. \tag{63}$$

Approaching the critical value $\Delta_0 = 3/2$ from below, ξ_0 diverges, which matches the absence of localization for $\Delta_0 > 3/2$, see Sec. II C 1. Thus, at $T = 0$, the system is in the strongly localized (bound) regime for $L > \xi_0$ and in the nonequilibrated regime (negligible effect of random tunneling) for $L < \xi_0$.

Let us now discuss what happens at finite temperature. As discussed in Sec. II C 1, the renormalization of disorder according to Eq. (55) (which physically results from an interaction-induced dressing of impurities) stops at the scale L_T. This gives a T-dependent mean free $\ell(T)$,

$$\ell(T) \sim \frac{L_T}{D(L_T)} \sim D_0^{-1} a (aT/v)^{2-2\Delta_0}. \tag{64}$$

This relation holds under the condition $D(L_T) < 1$ (or, equivalently, $\ell(T) > L_T$), i.e., for $T > T_0$, where

$$T_0 \sim a^{-1} v D_0^{1/(3-2\Delta_0)}. \tag{65}$$

For $T < T_0$ the mean free path $\ell(T)$ saturates at the value $\ell(0) = \xi_0$ given by Eq. (63).

As is clear from Eq. (65), the regime $\Delta_0 < 3/2$ is split into two subregimes with very different behavior: $\ell(T)$ increases with increasing T if $\Delta_0 < 1$, while it decreases with increasing T when $\Delta_0 > 1$. These two distinct cases are depicted in panels (a) and (b) of Fig. 2, respectively.

If the transport remains coherent up to the scale $\ell(T)$, the mean free path $\ell(T)$ becomes the (T-dependent) localization length $\xi(T) = \ell(T)$ as in usual disordered single-channel wires. The condition for strong localization is $\ell(T) < \ell_\varphi(T)$, where $\ell_\varphi(T)$ is the electron-electron scattering length [36],

$$\ell_\varphi(T) \sim \frac{1}{(\Delta_0 - 1)^2} L_T. \tag{66}$$

The factor $(\Delta_0 - 1)^{-2}$ is important close to the point $\Delta_0 = 1$, corresponding to noninteracting $+1$ and -1 modes, see Eq. (43). Away from the region $\Delta_0 = 1$, this factor can be replaced by unity. Thus, the strongly localized (i.e., bound) phase is realized for temperatures $T < T_B$, where the characteristic binding transition temperature T_B is determined by the condition $\ell(T) \sim \ell_\varphi(T)$, yielding

$$T_B \sim a^{-1} v \left[\frac{D_0}{(\Delta_0 - 1)^2}\right]^{1/(3-2\Delta_0)}. \tag{67}$$

For Δ_0 close to unity, the temperature T_B parametrically exceeds T_0 given by Eq. (65); otherwise, $T_B \approx T_0$.

For $T > T_B$, localization effects are reduced to a weak-localization correction to the conductivity. This correction is cut off by the weak-localization dephasing length $\ell_\varphi^{wl}(T) \sim [\ell_\varphi(T)\ell(T)]^{1/2}$ [36]. We will neglect this small correction in the present work. To the leading order, the transport in this situation is of classical character with the mean free path $\ell(T)$. In other words, $\ell(T)$ in this regime plays a role of the equilibration length ℓ_{eq}.

Summarizing, we have obtained the "phase diagram" of transport regimes for the case $\Delta_0 < 3/2$ as shown in Figs. 2(a) and 2(b). In these plots, a full line emanating from the point ξ_0 on the length axis is the T-dependent mean free path $\ell(T)$. For $T < T_B$, $\ell(T)$ constitutes the localization length $\xi(T)$, while for $T > T_B$ it becomes the equilibration length $\ell_{eq}(T)$.

(1) At lowest temperatures, $T \ll T_B$, and $L > \xi(T)$, the edge is in the strongly localized or bound phase (45). This is depicted as regime $\mathcal{I}$ in Figs. 2(a) and 2(b).

(2) For $L < \ell(T)$ for all T, disorder remains weak and no localization or equilibration occurs. We call this regime $\mathcal{II}$.

(3) For $T > T_B$ and $L > \ell_{eq}(T)$, dephasing suppresses the localization and, at the same time, the random tunneling leads to equilibration. This is regime $\mathcal{III}$.

The conclusion of the present analysis is that the bound phase is characterized by three transport regimes: the localization regime $\mathcal{I}$, and nonequilibrated and equilibrated regimes $\mathcal{II}$ and $\mathcal{III}$, respectively. This stands in stark contrast to the free phase which exhibit only regimes $\mathcal{II} - \mathcal{III}$. The existence of the localized regime is a striking manifestation of the fact that the $\nu = 9/5$ edge is T-unstable and thus susceptible to the binding transition. The localized regime $\mathcal{I}$ in the bound phase is depicted as the yellow regions in Fig. 2. With this phase diagram in mind, we now move on to a transport analysis for the regimes $\mathcal{I} - \mathcal{III}$.

III. TRANSPORT SIGNATURES OF THE BINDING TRANSITION

Electrical and thermal transport on FQH edges are usually quantized, reflecting a nontrivial bulk topological order [3]. Specifically, the electrical Hall and two-terminal conductances, G_H and G, are commonly proportional to the bulk filling factor [see Eq. (5)]

$$G_H = \nu \frac{e^2}{h}, \quad G = |G_H|. \tag{68}$$

By contrast, thermal Hall and two-terminal conductances, G_H^Q and G^Q are determined by ν_Q [see Eq. (6)] as

$$G_H^Q = \nu_Q \kappa T, \quad G^Q = \left|G_H^Q\right|, \tag{69}$$

where the heat conductance quantum $\kappa T = \pi^2 k_B^2 T/(3h)$, in which T is the temperature, and k_B and h are the Boltzmann and Planck constants, respectively.

For edges with counterpropagating channels, the quantizations (68) and (69) hold only in the transport regime of full edge channel equilibration [38,42]. To observe deviations from (68) and (69) requires poor equilibration, which can be achieved by very low temperatures, strong interchannel interactions [24,25], very small intercontact distance, or a detailed control over the interchannel tunneling strength [29]. Since ν_Q takes negative values on some edges (e.g., at filling $\nu = 3/5$), it has further been predicted that heat may flow in the opposite direction of the charge [33]. However, most experiments measure $|\nu_Q|$. It was therefore proposed that the direction of heat flow (i.e., the sign of ν_Q) is in direct correspondence with the scaling behavior of the electrical shot noise with the edge length L [39,43–46]. These insights have led to a deeper understanding of the FQH edge structure. In particular, recent measurements of the heat conductance [22,31] and noise [32] now strongly point towards GaAs/AlGaAs hosting the non-Abelian particle-hole-Pfaffian edge structure [47–50] at filling $\nu = 5/2$ [51,52].

As described in Sec. II, the binding transition preserves the topological transport coefficients ν and ν_Q. It is therefore clear that charge and heat conductances in the fully equilibrated regime cannot distinguish between the free (40) and bound (45) edge phases. Indeed, in both phases, the equilibrated transport coefficients are given as

$$G_H = G = \frac{9}{5}\frac{e^2}{h}, \tag{70}$$

$$G_H^Q = G^Q = 1\kappa T. \tag{71}$$

However, by building upon the results in Sec. II C, we will next argue that signatures of the binding transition can be deduced from edge transport experiments by accessing regimes with absent equilibration.

A. Two-terminal charge conductance

We first consider the two terminal charge conductance G [see Figs. 3(a) and 3(c)]. As follows, we assume for simplicity a sharp enough edge potential such that no edge reconstruction occurs. We also assume that in contact regions, screening causes the interchannel interactions to vanish.

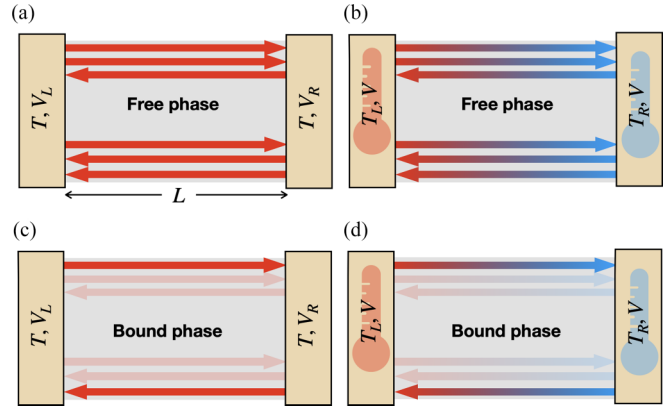

FIG. 3. Two-terminal setup for depicting edge transport at filling $\nu = 9/5$ in the free [(a) and (b)] and bound [(c) and (d)] edge phases. The device length is L. Two contacts at different potentials $V_L \neq V_R$ but the same temperature T allows extraction of the two-terminal conductance G (left figures). For contacts at the same potential $V_L = V_R = V$ but different temperatures $T_L \neq T_R$ (right figures), one can determine the two-terminal heat conductance G^Q.

1. The free phase

When the edge is in the free phase, $\Delta_0 > 3/2$, we expect with decreasing system size L and/or decreasing temperature T, a crossover in G. When $L \gg \ell_C$, i.e., for equilibration (i.e., regime $\mathcal{III}$, cf. Sec. II C), we expect $G/(e^2/h) = \nu = 9/5$ in accordance with Eq. (68). Since $\Delta_0 > 3/2$, we have from Eq. (61) that ℓ_C increases with decreasing T. When $L \sim \ell_C$, charge begins to propagate upstream, which increases G. In the limit of $L \ll \ell_C$, i.e., no equilibration (regime $\mathcal{II}$), the upstream channels transport charge upstream and also remain in equilibrium with the contact they were emitted from. The individual channel conductance contributions then add [38,53], i.e., $G/(e^2/h) = 1 + 1 + 1/5 = 11/5$. Hence, we expect the conductance characteristics

$$G/(e^2/h) = 11/5 \to 9/5, \tag{72}$$

with increasing L and/or T in the free edge phase. This corresponds to moving from the blue to the red region in Fig. 2(c).

2. The bound phase

In the localized regime $\mathcal{I}$, only a single channel transports charge over distances $L > \ell_C, \xi_0$. Hence, Eq. (68) gives the charge conductance $G/(e^2/h) = 9/5$. The analysis of regimes $\mathcal{II}$ and $\mathcal{III}$ proceed just as for the free phase and give charge conductances $G/(e^2/h) = 11/5$ and $G/(e^2/h) = 9/5$, respectively.

We next analyze two important situations. For $1 < \Delta_0 < 3/2$, Fig. 2(b) indicates that, for fixed $L > \ell_C, \xi_0$ the conductance remains at $G/(e^2/h) = 9/5$ with decreasing T, i.e., transitioning from regime $\mathcal{III}$ to regime $\mathcal{I}$. However, for $L < \ell_C, \xi_0$, the conductance increases from $G/(e^2/h) = 9/5$ to $11/5$ since one channel begins to conduct more and more charge upstream. The other case is $\Delta_0 < 1$, see Fig. 2(a). Just as in the previous case, a transition between regimes $\mathcal{I}$ and $\mathcal{III}$ is not visible in the charge conductance which remains at $G/(e^2/h) = 9/5$. This is the blue, dashed line in Fig. 2(a) However, we see that it is possible to crossover

directly between regimes $\mathcal{I}$ and $\mathcal{II}$. This is depicted as the red, dashed line. Such a transition would give rise to a change in the conductance

$$G/(e^2/h) = 11/5 \to 9/5, \tag{73}$$

with *decreasing* temperature, which is a quite unusual situation, only possible due to the existence of the localized regime. Observing this crossover would be a strong hallmark of edge localization and the binding transition.

B. Two-terminal heat conductance

Here, we consider the setup in Figs. 3(b) and 3(d) and analyze the two-terminal heat conductance $G^{\mathcal{Q}}$. We do note that state-of-the-art measurements of $G^{\mathcal{Q}}$ use a different geometry (see, e.g., Ref. [54]). This does not however change the validity of the results in this section.

In contrast to the topological quantization (69), in the regime of vanishing heat equilibration, $G^{\mathcal{Q}}$ becomes proportional to the total number of edge channels

$$G^{\mathcal{Q}} = (n_d + n_u)\kappa T. \tag{74}$$

This holds under the condition $L < L_T$ [55], which we assume is fulfilled as follows. Deviations from this assumption is commented upon below.

1. The free phase

Abelian FQH edge channels carry the same heat conductance regardless of their filling factor discontinuity $\delta\nu_i$ and charge t_i. Simple channel counting gives, for the free phase, the crossover

$$G^{\mathcal{Q}}/(\kappa T) = 3 \to 1. \tag{75}$$

with decreasing L and/or T. This corresponds to the two limiting values (69) and (74) when moving from regime $\mathcal{III}$ to $\mathcal{II}$. Analogously to the charge transport, the crossover is governed by a characteristic, nonuniversal, heat equilibration length ℓ_{Q}[$\sim\ell_{\mathrm{eq}}$ in Fig. 2(c)].

2. The bound phase

Also in the bound phase, we have in regime $\mathcal{III}$ a heat conductance $G^{\mathcal{Q}}/(\kappa T) = 1$ according to Eq. (69). In regime $\mathcal{II}$, Eq. (74) gives $G^{\mathcal{Q}}/(\kappa T) = 3$. For $1 < \Delta_0 < 3/2$, Fig. 2(b) indicates that, for fixed $L > \ell_{\mathrm{Q}}, \xi_0$ the heat conductance remains at $G^{\mathcal{Q}}/(\kappa T) = 1$ with decreasing T. For $L < \ell_{\mathrm{Q}}, \xi_0$, the heat conductance instead increases from $G^{\mathcal{Q}}/(\kappa T) = 1$ to $G^{\mathcal{Q}}/(\kappa T) = 3$. For strong interactions, $\Delta_0 < 1$, the transition between regimes $\mathcal{I}$ and $\mathcal{III}$ is not visible as $G^{\mathcal{Q}}/(\kappa T) = 1$ across the transition; the blue, dashed line in Fig. 2(a). Crossing over from $\mathcal{II}$ to $\mathcal{I}$ directly (the red, dashed line) yields the crossover

$$G^{\mathcal{Q}}/(\kappa T) = 3 \to 1, \tag{76}$$

with *decreasing* temperature, due to localization. Similarly to the charge conductance, such an unusual crossover is a hallmark of localization on the edge.

Finally, we comment on the situation $L > L_T$. Then, plasmon scattering on interfaces between edges and contacts lead to quantum interference effects [55,56]. This interference reduces the conductance from the value in Eq. (74). For example, the strongly interacting $\nu = 2/3$ edge with $L_T < L < \ell_{\mathrm{eq}}$ produces a heat conductance $G^{\mathcal{Q}}/(\kappa T) = 1$ [25,38]. A prerequisite for this interference effect is the presence of counterpropagating channels which do not thermally equilibrate. The only regime where the interference effect therefore could potentially have an impact is regime $\mathcal{II}$, where it would reduce $G^{\mathcal{Q}}/(\kappa T)$ from 3 to slightly lower values.

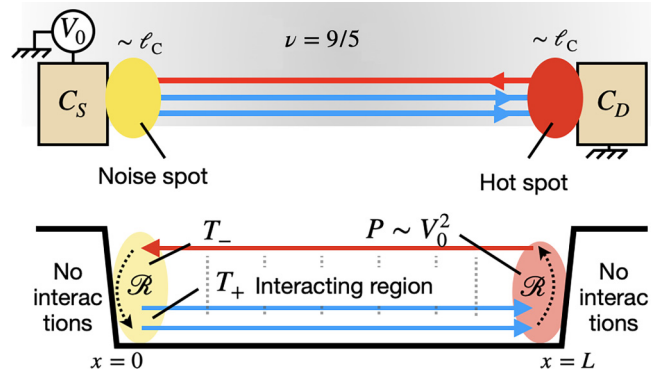

FIG. 4. (Top) Noise generation in regime of full charge equilibration but no thermal equilibration [condition (77)] in regime $\mathcal{II}$ (cf. Table I). With voltage bias V_0, heat is generated by the voltage dropping in a region of size $\sim\ell_{\mathrm{C}}$ to the *right* contact: the hot spot. The dissipated power $P \sim V_0^2$ [see Eq. (B16)]. Dc noise by partitioning of the downstream (left to right direction) charge current is only generated in a region of size $\sim\ell_{\mathrm{C}}$ close to the *left* contact. This happens if heat is transported upstream (right to left) via the upstream channel, which is here only possible in the absence of thermal equilibration. (Bottom) By dissipation in the hot spot and reflection of plasmons at contacts (reflection coefficient $\mathcal{R}$), the downstream and upstream modes acquire steady state temperatures T_+ respectively T_- in the noise spot.

C. Shot noise on a voltage biased edge segment

Here, we analyze the shot (or excess dc) noise, S, generated on a single edge segment, of length L, bridging two contacts (see Fig. 4). This setup was studied theoretically in Refs. [39,43–45] and has been realized experimentally for both conventional [26] and interfaced [32] edge structures.

Under conditions of strongly equilibrated charge transport, $\ell_{\mathrm{C}} \ll L$, noise in this setup is generated by an interplay between the charge and heat transport characteristics: when a charge current is driven between the two contacts, heat is generated only near the drain contact (in a region called the hot spot; see right hand side in Fig. 4). This is a consequence of downstream ballistic charge transport due to the efficient charge equilibration. By contrast, excess noise can only be generated near the source contact (in a region called the noise spot, see left hand side in Fig. 4) due to thermal enhancement of current partitioning. Partitioning beyond this spot leads, due to repeated charge scattering and the chiral nature of the edge, to scattered particles ending up in the same contact and no noise is generated. Nonzero shot noise in the contacts is therefore possible only if (i) the edge hosts

counterpropagating modes and (ii) there is an upstream heat flow from the hot spot to the noise spot.

Let us apply this reasoning to the $\nu = 9/5$ edge. In the localized regime $\mathcal{I}$, there is no upstream heat flow and therefore no noise; $S = 0$. In regime $\mathcal{III}$, the edge is fully thermally equilibrated and the upstream heat flow as well. The noise is then exponentially suppressed in L: $S \propto \exp[-L/\ell_C] \simeq 0$. These two regimes stand in stark contrast to regime $\mathcal{II}$, under the additional condition:

$$\ell_C \ll L \ll \ell_Q. \tag{77}$$

In this case, the edge has three charge equilibrated but not thermally equilibrated channels, conditions which have been experimentally observed [25,26]. Upstream heat transport is then possible. This heat reaches the noise spot through ballistic upstream flow and noise is generated. The condition (77) can arise due to strong interactions [24], so we expect that it holds only for $\Delta_0 \approx 0$, i.e., deep in the bound phase.

Our goal in the remainder of this subsection is to estimate the magnitude of S in regime $\mathcal{II}$, under the condition (77). In our analysis, we consider a large voltage bias $eV_0 \gg T$, which allows us to effectively set $T \approx 0$ in the following calculations.

The shot noise in any of the two contacts (see Fig. 4) (equal due to current conservation) can be written as [25]

$$S = \frac{2e^2}{h\ell_C}\frac{\nu_-}{\nu_+}(\nu_+ - \nu_-)\int_0^L dx\ \Lambda(x)e^{-\frac{2x}{\ell_C}}. \tag{78}$$

Here, ν_+ and ν_- are the combined filling factor discontinuities of the downstream (+) and upstream (−) edge modes, respectively. They satisfy the relation $\nu = \nu_+ - \nu_-$, where ν is the bulk filling factor. For the $\nu = 9/5$ edge in regime $\mathcal{II}$, we have $\nu_+ = 2$ and $\nu_- = 1/5$. The exponential factor in the integral is a result of chiral, equilibrated charge transport as described above. It indicates that noise is dominantly generated in a region of size $\sim l_{\rm eq}^C$ close to the upstream contact, i.e., the noise spot.

In Appendix B, we derive the following expression for the noise kernel $\Lambda(x)$ entering Eq. (78)

$$\Lambda(x) \approx \Lambda(T_\pm, \Delta) = \frac{\int dz \sin\left[\frac{T_+}{T_-}\left(\frac{\pi}{2}+iz\right)\right]^{-\delta_+}\cosh[z]^{-\delta_-}}{\int dz\left(\frac{1}{2T_-}+\frac{iz}{\pi T_-}\right)\sin\left[\frac{T_+}{T_-}\left(\frac{\pi}{2}+iz\right)\right]^{-\delta_+}\cosh[z]^{-\delta_-}}. \tag{79}$$

Here, the exponents

$$\delta_+ \equiv ((\tilde{\mathbf{m}}_1)_1)^2 + ((\tilde{\mathbf{m}}_1)_2)^2, \tag{80a}$$

$$\delta_- \equiv ((\tilde{\mathbf{m}}_1)_3)^2, \tag{80b}$$

$$\delta_+ + \delta_- = \Delta, \tag{80c}$$

and the edge eigenmode temperatures

$$k_B T_+ = \frac{3eV_0}{5\pi}\sqrt{\frac{\mathcal{R}(1+\mathcal{R})}{4-2\mathcal{R}^2}}, \tag{81a}$$

$$k_B T_- = \frac{3eV_0}{5\pi}\sqrt{\frac{1+\mathcal{R}}{2-\mathcal{R}^2}}. \tag{81b}$$

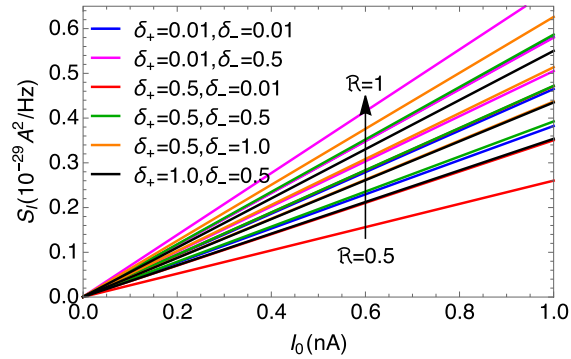

FIG. 5. Noise S vs the bias current I_0 for different values of the scaling dimensions $\delta_\pm$ [see Eq. (B14)] and the edge contact reflection coefficient $\mathcal{R}$. The calculation is done for the $\nu = 9/5$ edge under the condition (77) for the edge equilibration length scales.

Here, we have assssumes that all downstream modes have the temperature T_+, and the upstream modes are at T_-. Furthermore, $\mathcal{R} \in [0, 1]$ is the reflection coefficient between the contacts and the edge. Using the expressions $\nu_+ = 2$ and $\nu_- = 1/5$, Eq. (78) can be written as

$$S = \frac{9e^2}{50h}\Lambda(T_\pm, \Delta). \tag{82}$$

For simpler comparison with the experimental convention of plotting S versus the source current I_0, we next convert the bias voltage V_0 to I_0 via

$$I_0 = \frac{9}{5}\frac{e^2}{h}V_0, \tag{83}$$

which is valid under the condition (77).

We now have all ingredients to compute the noise in Eq. (82) for a given bias current I_0. We evaluate the integrals in Eq. (79) numerically for various values of $\mathcal{R}$ and $\delta_\pm$ and plot the result in Fig. 5. Since we expect the condition (77) to be obtained for strong interactions which also tend to increase $\mathcal{R}$, we limit the range of $\mathcal{R}$ to the range $\mathcal{R} \in [0.5, 1]$, for consistency. For experimental comparison, we have reinstated experimentally convenient units where noise is measured in 10^{-29} A^2/Hz and currents in nano ampere. Qualitatively, we see that for fixed $\mathcal{R}$, the dependencies on $\delta_\pm$ are quite weak, whereas the dependence on $\mathcal{R}$ is pronounced. This can be understood on physical grounds since $\mathcal{R}$ strongly affects the temperatures $T_\pm$ at the noise spot. By inspection, we give the rough estimate

$$S \approx 0.25 - 0.7 \times 10^{-29}\frac{\text{A}^2}{\text{nA Hz}}. \tag{84}$$

This magnitude is around half of that detected for the $\nu = 2/3$ edge in Ref. [26]. The noise in regime $\mathcal{II}$ should therefore be detectable with present technology.

D. Shot noise in a QPC device

As a complement to the transport characteristics in previous subsections, we here compute the electrical shot noise generated by current partitioning in a QPC device [57–60]. We consider both the WBS regime [see Figs. 6(a) and 6(c)], allowing tunneling of fractionally charged quasiparticles through

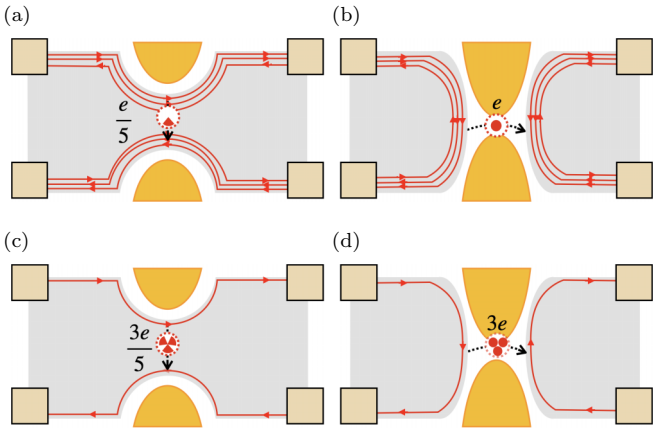

FIG. 6. Schematics of a quantum point contact (QPC) device at filling $\nu = 3/5$. [(a) and (b)] In the free phase, the weak back-scattering (WBS) regime favours tunneling of quasiparticles with charge $e/5$. For strong back-scattering (SBS), electrons with charge e tunnel. (c) In the bound phase, the WBS regime is dominated by tunneling of fractional charges $3e/5$. (d) In the SBS regime in the bound phase, single electron tunneling is strongly suppressed at low energies and three electron cotunneling, i.e., charge packets of $3e$ is the most dominant process. All four types of charges can be detected in shot noise measurements.

the FQH bulk, and the SBS regime, which only allows electron tunneling across the nontopological vacuum [Figs. 6(b) and 6(d)].

In this section, we present formulas for the tunneling current, shot noise, Fano factor, and tunneling conductance in point tunneling between two counterpropagating edge channels. Details in the derivation are given in Appendix C. We then apply these formulas to obtain Fano factors for the bound and free phases, in both SBS and WBS regimes. We follow closely the perturbative Keldysh approach from Refs. [42,53,61].

1. QPC model and formulas for tunneling current and noise

The edge channels in the QPC device is described by the effective Hamiltonian

$$H_0 = \pi \int dx \left[v_1 \frac{\rho_1^2}{t_1^2} + v_2 \frac{\rho_2^2}{t_2^2} \right], \tag{85}$$

where $\rho_i = t_i \partial_x \phi_i/(2\pi)$ $(i = 1, 2)$ are the neigbouring two counterpropagating charge densities (with velocities v_i) on each side of the constriction. For simplicity, we ignore the fully transmitted or reflected channels in the free phase. Their influence in the form of interchannel interactions are discussed below Eq. (94) and in Appendix C below Eqs. (C18) and (C20). We further ignore all interactions across the constriction. The bosons ϕ_i and their densities obey the following set of commutation relations:

$$[\phi_i(x), \phi_j(x')] = i\pi \delta_{ij} \delta\nu_i \, \mathrm{sgn}(x - x'), \tag{86}$$

$$[\rho_i(x), \rho_j(x')] = \frac{i}{2\pi} \delta_{ij} t_i^2 \delta\nu_i \partial_x \delta(x - x'), \tag{87}$$

$$[\phi_i(x), \rho_j(x')] = i\delta_{ij} t_i \delta\nu_i \delta(x - x'). \tag{88}$$

Here, the filling factor discontinuities $\delta\nu_i$ and the charge vector entries t_i are kept unspecified for full generality. To describe charge tunneling in the presence of a voltage bias, we introduce chemical potentials and point tunneling (at position $x = 0$) with

$$H_V = -\int dx [\mu_1 \rho_1 + \mu_2 \rho_2], \tag{89}$$

$$H_\tau = \int dx \delta(x) [\Gamma_0 \mathcal{T}_{\mathbf{l}}(x) + \text{H.c.}]. \tag{90}$$

Here, Γ_0 is the tunneling amplitude and

$$\mathcal{T}_{\mathbf{l}}(x) = \frac{e^{il_1\phi_1(x) + il_2\phi_2(x)}}{2\pi a}, \tag{91}$$

is a tunneling operator parametrized by $\mathbf{l} = (l_1, l_2)$ [cf. Eq. (7)]. The length a is our UV distance cutoff, e.g., the magnetic length. According to Eq. (9), the charge created by $e^{il_1\phi_1}$ is

$$q_1 = t_1 \delta\nu_1 l_1. \tag{92}$$

Similarly, $e^{il_2\phi_2}$ creates charge

$$q_2 = t_2 l_2 \delta\nu_2. \tag{93}$$

Conservation of charge in the tunneling process restricts l_1 and l_2 such that

$$q_1 = q_2 \equiv q \tag{94}$$

for a given set $\{t_1, t_2, \delta\nu_1, \delta\nu_2\}$. Note that since Eq. (9) is invariant under basis rotations, the charges q_1, q_2, and q are all independent of possible interactions with fully transmitted and reflected channels in the free phase.

In Appendix C, we present our calculation of the average QPC tunneling current $\langle I \rangle$ and zero frequency noise $S(\omega = 0)$. They are given as

$$\langle I \rangle \equiv \langle I(t) \rangle = 2q|\Gamma_0|^2 (2\pi a)^{2\Delta(\mathbf{l})-2} T^{2\Delta(\mathbf{l})-1} \times \prod_k \left(\frac{1}{v_k} \right)^{2d_k} \sinh\left(\frac{\omega_0}{2T} \right) \frac{\left| \Gamma\left(\Delta(\mathbf{l}) + i\frac{\omega_0}{2\pi T} \right) \right|^2}{\Gamma(2\Delta(\mathbf{l}))} \tag{95}$$

and

$$S(\omega = 0) = 2q \cosh\left(\frac{\omega_0}{2T} \right) \frac{\langle I \rangle}{\sinh\left(\frac{\omega_0}{2T} \right)} = 2q \langle I \rangle \coth\left(\frac{\omega_0}{2T} \right). \tag{96}$$

In Eqs. (95) and (96), the parameter

$$\omega_0 \equiv (t_1 l_1 \delta\nu_1 \mu_1 - t_2 l_2 \delta\nu_2 \mu_2) = q(\mu_1 - \mu_2) \tag{97}$$

is a characteristic frequency of the tunneling, and

$$\Delta(\mathbf{l}) = \tfrac{1}{2}\left(|\delta\nu_1| l_1^2 + |\delta\nu_2| l_2^2 \right), \tag{98}$$

is the scaling dimension of the tunneling operator $\mathcal{T}_{\mathbf{l}}$ in Eq. (91). In the shot-noise limit $\omega_0 \gg T$, the Fano factor

$$F \equiv \frac{S(\omega = 0)}{2\langle I \rangle} = q \coth\left(\frac{\omega_0}{2T} \right) \xrightarrow[\omega_0 \gg T]{} q. \tag{99}$$

reveals the charge in the tunneling process. In the limit $\omega_0 \ll T$, the tunneling current can be written on Ohmic form

as $\langle I\rangle = g_\tau e^2(V_1 - V_2)/h$ with $eV_1 = \mu_1$, $eV_2 = \mu_2$, and the tunneling conductance

$$g_\tau \equiv q^2 \frac{|\Gamma_0|^2(2\pi aT)^{2\Delta(\mathbf{l})-2}}{\prod_k v_k^{2d_k}} \frac{|\Gamma(\Delta(\mathbf{l}))|^2}{\Gamma(2\Delta(\mathbf{l}))}. \tag{100}$$

Next, we use the charges (92)–(94), the scaling dimensions (98), the Fano factor (99), and the tunneling conductance (100) to analyze tunneling in the free and bound edge phases.

2. Fano factors for the free phase

For a $\nu = 9/5$ device in the free phase, we have for the innermost channels $t_1 = t_2 = 1$ and $\delta\nu_1 = -\delta\nu_2 = 1/5 \equiv \delta\nu$ [see Eq. (40)]. In the WBS regime, fractional charges may tunnel across the constriction through the Hall fluid, and, as stated above, the most relevant tunneling operator $\mathcal{T}_\mathbf{l}$ is obtained for $l_1 = l_2 = l = 1$. The operator then describe the transfer of particles with charge

$$q = t\delta\nu l = 1 \times \tfrac{1}{5} \times 1 = \tfrac{1}{5}. \tag{101}$$

Using Eqs. (98) in Eq. (100), we see that the tunneling conductance for this process scales with temperature in the Ohmic limit as $g_\tau \sim T^{-8/5}$. Note that this scaling law strictly holds in the absence of interactions. However, interactions are expected to only lead to small deviations from this value of the scaling exponent. The divergence at zero temperature signals the instability of the system towards quasiparticle tunneling. Thus, this type of tunneling is only visible at high temperatures/voltages.

In the SBS regime, the left and right parts of the constriction are bridged by a region fully depleted of Hall fluid. No FQH quasiparticles may exist in this region, and hence only tunneling processes of electrons (integer charges) couple the edges. The most dominant such process is obtained for $l = 5$, which gives a smallest possible integer charge of

$$q = t\delta\nu l = 1 \times \tfrac{1}{5} \times 5 = 1, \tag{102}$$

i.e., single electron tunneling. For this process, Eqs. (98) and (100) show that the tunneling conductance scaling with temperature becomes in the Ohmic limit $g_\tau \sim T^8$. Also this scaling exponent may be modified by interactions but we expect this effect to be small. The SBS regime is a stable RG fixed point.

Direct application of Eq. (99) for these two types of processes give the Fano factors for the free phase

$$F_{\mathrm{WBS}} = \tfrac{1}{5}, \tag{103}$$

$$F_{\mathrm{SBS}} = 1. \tag{104}$$

From these results, we predict that in the free phase, shot noise measurements in the WBS and SBS regimes should reveal tunneling of fractional charges $q = 1/5$ and single electrons $q = 1$, respectively.

3. Fano factors for the bound phase

In the bound phase, we have $t_1 = t_2 = 3$ and $\delta\nu_1 = -\delta\nu_2 = 1/5$ [see Eq. (45)]. In the WBS regime, the most relevant tunneling operator is again obtained for $l = 1$, which amounts to transfer of particles with charge

$$q = t\delta\nu l = 3 \times \tfrac{1}{5} \times 1 = \tfrac{3}{5}. \tag{105}$$

In the SBS regime, we seek the most relevant operator transferring an integer number of charges. From Eq. (92), we see that, once more, this operator is found for $l = 5$, which amounts to the tunneling of charge

$$q = t\delta\nu l = 3 \times \tfrac{1}{5} \times 5 = 3. \tag{106}$$

The conductance scaling laws in the WBS and SBS regimes are $g_\tau \sim T^{-8/5}$ and $g_\tau \sim T^8$, respectively, i.e., the same as those obtained for the bound phase. Application of Eq. (99) for the WBS and SBS regimes gives

$$F_{\mathrm{WBS}} = \tfrac{3}{5}, \tag{107}$$

$$F_{\mathrm{SBS}} = 3. \tag{108}$$

Equation (108) is a key result of this section. It signals three-electron co-tunneling as the most relevant process in the SBS regime. Since, $t_1 = t_2 = t = 3$, a process yielding $F_{\mathrm{SBS}} = 1$ is impossible at low energies in the bound phase. Similarly, for WBS, it not possible to observe particles with charge $1/5$ in the bound phase. Measuring $F_{\mathrm{SBS}} = 3$ and $F_{\mathrm{WBS}} = 3/5$ in the SBS respectively WBS regimes, is therefore a striking manifestation of the $9/5$ edge in the bound phase.

4. Tunneling between the bound edge and a metal

As a consistency check of our equations, we consider finally also the previously studied setup [18] of electron tunneling from an ordinary metal (or, equivalently, an integer quantum Hall edge) into the bound $9/5$ edge. As previously stated, only tunneling of electrons in bunches of three is possible. We therefore have $t_1 = 1$, $\delta\nu_1 = 1$, and $l_1 = 3$, respectively $t_2 = 3$, $\delta\nu_2 = -1/5$, and $l_2 = 5$. Since $q_1 = t_1|\delta\nu_1|l_1 = q_2 = t_2|\delta\nu_2|l_2 = 3$, we immediately find from Eq. (99) that $F = 3$ for this tunneling. Furthermore, Eq (98) gives the scaling dimension

$$\Delta = \tfrac{1}{2}\left(1 \times 3^2 + \tfrac{1}{5} \times 5^2\right) = 7, \tag{109}$$

for the most relevant tunneling operator. It follows that in the high-temperature limit, Eq. (100) gives that the tunneling conductance scales as $g_\tau \sim T^{2\Delta-2} = T^{12}$. In the low-temperature limit, we have from dimensional analysis $\langle I\rangle \sim V^{2\Delta-1} = V^{13}$. These scaling laws are precisely those derived in Ref. [18].

We end Sec. III by summarizing the key results in Table I.

IV. DISCUSSION

Our analysis at $\nu = 9/5$ can straightforwardly be adapted to other T-unstable edge structures (several examples were given in Ref. [18]). Consider for example an interface between bulk fillings $\nu = 2/5$ and $1/7$. Here, we assume that a FQH state and not a Wigner crystal forms at filling $\nu = 1/7$ of the electron gas.

The resulting edge structure is described by

$$K = \begin{pmatrix} 3 & 0 & 0 \\ 0 & 15 & 0 \\ 0 & 0 & -7 \end{pmatrix}, \quad \mathbf{t}^T = (1, 1, 1). \tag{110}$$

According to Eq. (5), the "effective filling" of this structure is $\nu = 9/35$. The two null vectors are $\mathbf{m}_1 = (1, 10, 7)^T$ and $\mathbf{m}_2 = (4, -5, 7)^T$. Crossing over from the corresponding regimes $\mathcal{III}$ to $\mathcal{II}$, we therefore expect conductance transitions $G = 9/35 \to 19/35$ and $G^Q = 1 \to 3$ with decreasing temperature.

A basis transformation of Eq. (110) on the form (15) leads to an alternative representation

$$K' = \begin{pmatrix} 35 & 0 & 0 \\ 0 & 1 & 0 \\ 0 & 0 & -1 \end{pmatrix}, \quad \mathbf{t}'^{\mathbf{T}} = (3, 1, 1). \tag{111}$$

The binding transition amounts to the pair of counterpropagating integer channels localizing. The remaining channel has a filling factor discontinuity $\delta\nu = 1/35$ and it is made out of $3e$ composites. Hence, the bound phase is characterized by

$$K' = (35), \quad \mathbf{t}'^{\mathbf{T}} = (3). \tag{112}$$

In the bound phase, we therefore expect conductances $G = 9/35$ and $G^Q = 1$ in regime $\mathcal{I}$.

Tunneling in a QPC bridging two interfaced edges is geometrically complicated and we do not analyze it here. However, electron tunneling into the interface edge from a metal (e.g., an STM tip or a $\nu = 1$ QH state) is conceptually simpler and we use Eq. (98) to compute the scaling dimension of the tunneling operator (7) transferring three electrons. The result is

$$\Delta = \tfrac{1}{2}\left(1 \times 3^2 + \tfrac{1}{35} \times 35^2\right) = 22, \tag{113}$$

where we used $t_1 = 1$, $\delta\nu_1 = 1$, and $l_1 = 3$, respectively $t_2 = 3, \delta\nu_2 = -1/35$, and $l_2 = 35$. Then, from Eqs. (92), (93), and (94), we have $q_1 = t_1|\delta\nu_1|l_1 = q_2 = t_2|\delta\nu_2|l_2 = 3$. With these values, Eq. (99) produces $F = 3$ as expected for this tunneling. From Eq. (100), we have that the tunneling conductance scales with temperature as $g_\tau \sim T^{2\Delta-2} = T^{42}$. In the low-temperature limit, the voltage scaling of the current reads $\langle I \rangle \sim V^{2\Delta-1} = V^{41}$. We note here that a common property of electronic tunneling into a bound FQH edge are the unusually large conductance scaling exponents. Extracting these scaling exponents accurately may be prone to experimental difficulties. Nonetheless, we believe that large scaling exponents are important cues to look for in detecting FQH binding transitions.

We now move on to discuss practical aspects of experimentally detecting the binding transition. The transition at filling $\nu = 9/5$ can be expected to require tunneling between Landau levels with different spin polarization. Breaking spin-rotation symmetry, for example by spin-orbit coupling, is therefore a necessary condition. A bilayered device could be used to facilitate the binding transition [18]. Alternatively, carefully designed devices in the spirit of Ref. [29] where all channels have the same spin may be another possibility.

In our view, the most standard probe of the binding transition should be a measurement of the shot noise in a QPC device. From Sec. III D, we anticipate that, with decreasing temperature, a binding transition at $\nu = 9/5$ amounts to the crossover from $F_{\mathrm{SBS}} = 1$ to 3 in the strong back-scattering regime of the QPC. Similarly, for weak back-scattering, one expects a crossover from $F_{\mathrm{WBS}} = 1/5$ to $3/5$. Changes in Fano factors with decreasing temperature were recently measured in Ref. [62]. It would be interesting to investigate whether these changes could arise due to a combination of edge reconstruction and binding transitions.

V. SUMMARY AND OUTLOOK

We proposed quantum transport signatures for the FQH edge binding transition, with focus on filling $\nu = 9/5$. For this edge, we showed that interactions and disorder conspire to generate a rich phase diagram (Fig. 2) with distinct charge and heat transport regimes (see Table I). The three regimes, labeled $\mathcal{I}$, $\mathcal{II}$, and $\mathcal{III}$ displays localized, nonequilibrated, and fully equilibrated characteristics. Probing the distinct transport behavior, in terms of charge and heat conductances, of these regimes should be possible with present technology. As a complement to the conductance, we also estimated the shot noise produced of a single current biased edge segment. We demonstrated that such noise is only expected for the thermally nonequilibrated edge (regime $\mathcal{II}$) under the strong interaction condition (77) associated with the bound phase.

We also studied a QPC device in the strong and weak backscattering regimes and derived shot noise Fano factors for tunneling processes across the constriction. The bound phase does not allow single electron tunneling in the strong back-scattering (SBS) regime. Instead of the typical Fano factor $F_{\mathrm{SBS}} = 1$ corresponding to single electron tunneling, we therefore found that the smallest Fano factor compatible with transferring an integer number of charges is $F_{\mathrm{SBS}} = 3$. This corresponds to three-electron co-tunneling. In addition, all higher order (but less relevant) tunneling processes of electrons are necessarily integer multiples of 3. In the weak back-scattering (WBS) regime, we found that the most relevant tunneling of quasiparticles yields $F_{\mathrm{SBS}} = 3/5$. These SBS and WBS Fano factors are in stark contrast to those for the free phase: $F_{\mathrm{SBS}} = 1$ respectively $F_{\mathrm{WBS}} = 1/5$. These contrasting values serve as a clear signature for the binding transition.

We hope that our predictions and proposals will stimulate further theoretical and experimental investigations of FQH binding transitions. While our present analysis focused on Abelian FQH edges, binding transitions for non-Abelian candidate edge theories for the state filling $\nu = 5/2$ were studied in Ref. [63]. An experimentally oriented analysis similar to the present work could be useful for pin-pointing that state's underlying topological order.

ACKNOWLEDGMENTS

C.S. thanks Jinhong Park, Gu Zhang, and Kyrylo Snizhko for discussions. C.S. and A.D.M acknowledge support from the DFG Grant No. MI 658/10-2 and the German-Israeli Foundation Grant No. I-1505-303.10/2019. C.S. further acknowledge funding from the EI Nano Excellence Initiative at Chalmers University of Technology. This project has received funding from the European Union's Horizon 2020 research and innovation programme under Grant Agreement No. 101031655 (TEAPOT). This work was also supported by the European Union's Horizon 2020 research and innovation programme (Grant Agreement No. LEGOTOP No. 788715),

the DFG (CRC/Transregio 183, EI 519/7-1), ISF Quantum Science and Technology (2074/19).

APPENDIX A: DIMENSIONS OF THE DISORDER STRENGTH D

A generic tunneling operator $\mathcal{T}_{\mathbf{l}}$ has length (L) dimensions

$$L^{-m/2}, \tag{A1}$$

where m is the number of involved vertex operators ($m = 3$ for the $\nu = 9/5$ edge). The action (10) is dimensionless, so the random tunneling amplitude $\xi(x)$ has dimensions

$$L^{m/2-1}s^{-1}. \tag{A2}$$

where s is the unit of time. From Eq. (28), we then have that the units of D are

$$L^{m-1}s^{-2}. \tag{A3}$$

Hence, to obtain a dimensionless D we let

$$D \to D \times \frac{a^{3-m}}{v^2}, \tag{A4}$$

with some characteristic velocity v (a combination of all v_i to various powers such that the total power is 2). This result is consistent with Ref. [35] in which $m = 2$.

APPENDIX B: CALCULATION OF THE NOISE KERNEL

In Eq. (78), the noise generated along an edge segment (see Fig. 4) is given as

$$S = \frac{2e^2}{h\ell_C}\frac{v_-}{v_+}(v_+ - v_-)\int_0^L dx\ \Lambda(x)e^{-\frac{2x}{\ell_C}}. \tag{B1}$$

The key quantity to compute in Eq. (B1) is the local noise kernel

$$\Lambda(x) \equiv \frac{S_{\rm loc}[\delta V(x), T_+(x), T_-(x), \Delta]}{2g_{\rm loc}[\delta V(x), T_+(x), T_-(x), \Delta]}. \tag{B2}$$

It is composed of $S_{\rm loc}$ and $g_{\rm loc}$ which is the local electron tunneling dc noise and the (dimensionless) tunneling conductance, respectively. Importantly, the conductance $g_{\rm loc} \propto \ell_C^{-1}$, where the proportionality factor is the typical distance between scattering points [40,43]. Both $S_{\rm loc}$ and $g_{\rm loc}$ depend on microscopic details of the edge: interchannel interactions, the edge disorder strength, the local voltage difference between the modes $\delta V(x)$, and the effective temperatures $T_\pm(x)$ of downstream and upstream edge modes. Importantly, the interactions enter via the scaling dimension Δ of the most relevant interchannel charge tunneling operator (7).

Under the condition $\ell_C \ll L \ll \ell_Q$ [given in Eq. (77)], both the voltage difference and the temperatures are to excellent approximation constant across the noise spot:

$$\delta V(x) \approx 0 \quad \text{and} \quad T_\pm(x) \approx T_\pm. \tag{B3}$$

The first approximation holds because the channels equilibrate to the same voltage along the edge (except at the hot spot), whereas the second holds because of assumed poor thermal equilibration. With the approximations (B3), we can write

$$\Lambda(x) \approx \Lambda(T_\pm, \Delta). \tag{B4}$$

By using Eq. (B4) in Eq. (B1), the integral can be trivially performed to give

$$S = \frac{9e^2}{50h}\Lambda(T_\pm, \Delta). \tag{B5}$$

We now want to find $\Lambda(T_\pm, \Delta)$. The first step is to specify the edge tunneling operator, which we take as the null operator (42) with $\mathbf{m}_1$ from Eq. (41). We use the basis (40).

For this tunneling process, we next compute $\Lambda(T_\pm, \Delta)$ with the approach described in Ref. [26] (see also Appendix C for similar calculations). For weak tunneling, a perturbative approach for the local noise and conductance gives

$$S_{\rm loc} \propto 2\int dt\ \cos(\delta V t)\langle \mathcal{V}_{\mathbf{m}_1}(t,0)\mathcal{V}^\dagger_{\mathbf{m}_1}(0,0)\rangle \tag{B6}$$

$$g_{\rm loc} \propto i\partial_{\delta V}\left[\int dt\ \sin(\delta V t)\langle \mathcal{V}_{\mathbf{m}_1}(t,0)\mathcal{V}^\dagger_{\mathbf{m}_1}(0,0)\rangle\right]_{\delta V\to 0}. \tag{B7}$$

Here, the nonuniversal proportionality constant depends on a short distance cutoff, but importantly, the constant is the same for $S_{\rm loc}$ and $g_{\rm loc}$ and therefore cancels in Λ. Inserting the above expressions into Eq. (B2) and using $\delta V = 0$ gives

$$\Lambda(T_\pm, \Delta) = \frac{\int dt\ \langle \mathcal{V}_{\mathbf{m}_1}(t,0)\mathcal{V}^\dagger_{\mathbf{m}_1}(0,0)\rangle}{i\int dt\ t\langle \mathcal{V}_{\mathbf{m}_1}(t,0)\mathcal{V}^\dagger_{\mathbf{m}_1}(0,0)\rangle}. \tag{B8}$$

In Eq. (B8), the temperature dependence enters via the correlation functions

$$\langle \mathcal{V}_{\mathbf{m}_1}(t,0)\mathcal{V}^\dagger_{\mathbf{m}_1}(0,0)\rangle \propto \prod_{j=1,2,3}\tilde{G}_j(t,0)^{((\tilde{\mathbf{m}}_1)_j)^2}, \tag{B9}$$

where the finite temperature Green's functions

$$\tilde{G}_j(t,0) = \frac{\pi a T_j/\tilde{v}_j}{\sin\left[\frac{\pi T_j}{\tilde{v}_j}(a - i\tilde{v}_j t)\right]}, \quad j \in \{1,2,3\}, \tag{B10}$$

Note that the Green's functions are those of the modes in the diagonal basis (14). From Eq. (25), we have that the exponents in (B9) satisfy

$$((\tilde{\mathbf{m}}_1)_1)^2 + ((\tilde{\mathbf{m}}_1)_2)^2 + ((\tilde{\mathbf{m}}_1)_3)^2 = 2\Delta. \tag{B11}$$

The formula for the noise (B1) assumes that all downstream modes have the temperature T_+, and the upstream modes are at T_-. We thus set

$$T_1 = T_2 = T_+, \tag{B12a}$$

$$T_3 = T_-. \tag{B12b}$$

By plugging these temperatures into the Green's functions (B10), and expanding to leading order in a, we can cast Eq. (B8) on the form

$$\Lambda(T_\pm, \Delta) = \frac{\int dz \sin\left[\frac{T_+}{T_-}\left(\frac{\pi}{2} + iz\right)\right]^{-\delta_+}\cosh[z]^{-\delta_-}}{\int dz\left(\frac{1}{2T_-} + \frac{iz}{\pi T_-}\right)\sin\left[\frac{T_+}{T_-}\left(\frac{\pi}{2} + iz\right)\right]^{-\delta_+}\cosh[z]^{-\delta_-}}, \tag{B13}$$

where the exponents

$$\delta_+ \equiv ((\tilde{\mathbf{m}}_1)_1)^2 + ((\tilde{\mathbf{m}}_1)_2)^2, \tag{B14a}$$

$$\delta_- \equiv ((\tilde{\mathbf{m}}_1)_3)^2. \tag{B14b}$$

Our next step is to find $T_\pm$ in terms of the bias voltage V_0. When n_+ downstream and n_- upstream edge modes are not thermally equilibrated, the local downstream and upstream temperatures at the noise spot, $T_\pm$, were computed in Ref. [26]. They are given as

$$k_B T_+ = \left(\frac{6hP}{\pi^2} \times \frac{\mathcal{R}(n_- + \mathcal{R})}{(n_+ + n_-)(n_+ n_- - \mathcal{R}^2)}\right)^{1/2}, \tag{B15a}$$

$$k_B T_- = \left(\frac{6hP}{\pi^2} \times \frac{n_+(n_- + \mathcal{R})}{(n_+ + n_-)(n_+ n_- - \mathcal{R}^2)}\right)^{1/2}. \tag{B15b}$$

Here $\mathcal{R} \in [0, 1]$ is the reflection coefficient between the contacts and the edge. This reflection depends explicitly on the sharp change in interaction strength between the contact region and the edge [26,38,53] (see Fig. 4). We have assumed that both contacts have the same $\mathcal{R}$. Eq. (B15) also includes P, the power dissipated in the hot spot, which was computed in Ref. [44] as

$$P = \frac{e^2 V_0^2}{2h} \times \frac{(\nu_+ - \nu_-)\nu_-}{\nu_+}, \tag{B16}$$

under the assumption (77). For the $\nu = 9/5$ edge in regime $\mathcal{II}$, we have $\nu_+ = 2$, $\nu_- = 1/5$, $n_+ = 2$, and $n_- = 1$. Plugging these numbers into Eqs. (B15) and (B16), we find

$$P = \frac{9e^2 V_0^2}{100h}, \tag{B17}$$

and

$$k_B T_+ = \frac{3eV_0}{5\pi}\sqrt{\frac{\mathcal{R}(1+\mathcal{R})}{4 - 2\mathcal{R}^2}}, \tag{B18a}$$

$$k_B T_- = \frac{3eV_0}{5\pi}\sqrt{\frac{1+\mathcal{R}}{2 - \mathcal{R}^2}}. \tag{B18b}$$

For $\mathcal{R} = 0$, which corresponds to vanishing edge interactions, we have $k_B T_+ = 0$ and $k_B T_- = 3eV_0/(5\pi\sqrt{2})$. This is the situation where the downstream channels remain in equilibrium with the left contact (in our approximation, at $T = 0$) and only the upstream channel is heated by dissipation at the hot spot. Even in the absence of thermal equilibration by edge impurities, a finite reflection probability at the two contacts distributes the hot spot power to all edge channels.

APPENDIX C: DERIVATION OF QPC OBSERVABLES

To compute the tunneling current, we begin by defining the channel i current operator as

$$I_i = \frac{d}{dt}\left(\int dx \rho_i\right) = \frac{1}{i}\left[\int dx \rho_i, H_0 + H_V + H_\tau\right] = \frac{1}{i}\left[\int dx \rho_i, H_\tau\right], \tag{C1}$$

where we used that ρ_i commutes with the quadratic H_0 and H_V. The commutator with H_τ yields

$$I_1 = -I_2 \equiv I = iq\Gamma_0 \mathcal{T}_\mathbf{l}(0) + \text{H.c.} \tag{C2}$$

In the interaction picture with H_τ as the interaction Hamiltonian, any operator A time-evolves as

$$A(t) = e^{i(H_0+H_V)t} A e^{-i(H_0+H_V)t}. \tag{C3}$$

Applying this formula to operators I and H_τ, we find the time evolutions

$$H_\tau(t) = e^{-i\omega_0 t}\Gamma_0 \mathcal{T}_\mathbf{l}(0) + \text{H.c.}, \tag{C4a}$$

$$I(t) = iqe^{-i\omega_0 t}\Gamma_0 \mathcal{T}_\mathbf{l}(0) + \text{H.c.}, \tag{C4b}$$

where the characteristic "Josephson frequency" of the tunneling process

$$\omega_0 \equiv (t_1 l_1 \delta\nu_1 \mu_1 - t_2 l_2 \delta\nu_2 \mu_2) = q(\mu_1 - \mu_2). \tag{C5}$$

In the second equality here, we used the charge conservation condition (94). The relation between ω_0 and the voltage across the constriction reads $\hbar\omega_0 = qe(V_1 - V_2)$.

Next, we compute the expectation value of the current $\langle I(t)\rangle$ on the Keldysh contour

$$\langle I(t)\rangle = \frac{1}{2}\sum_{\lambda=\pm1}\left\langle T_C\left[I(t^\lambda)\exp\left(-i\int_C dt_0 H_\tau(t_0^{\lambda'})\right)\right]\right\rangle. \tag{C6}$$

Here, the Keldysh time-ordering operator, T_C orders along the Keldysh contour C: $-\infty \to +\infty \to -\infty$. We denote the "upper" branch $-\infty \to +\infty$ by $\lambda = +1$ and "lower" branch $+\infty \to -\infty$ with $\lambda = -1$. The ordering acts according to $t^- > t_0^+$ for all t and t_0; $t^+ > t_0^+$ for $t > t_0$; and $t^- > t_0^-$ for $t < t_0$. Since our H_τ only depends on a single time argument, we have used a symmetric combination on both branches, compensated for with the factor of $1/2$.

To second order in Γ_0, we find

$$\langle I(t)\rangle = \frac{q|\Gamma_0|^2}{2}\sum_{\lambda,\lambda'=\pm1}\lambda'\int_{-\infty}^{\infty} dt_0 \sin\left[\omega_0(t^\lambda - t_0^{\lambda'})\right] \times \langle T_C \mathcal{T}_\mathbf{l}(0, t^\lambda)\mathcal{T}_\mathbf{l}^\dagger(0, t_0^{\lambda'})\rangle, \tag{C7}$$

where we used that the tunneling operators are normal ordered. Next, we use the finite temperature Keldysh Green's functions for the tunneling operators

$$\left\langle T_C \mathcal{T}(0, t^\lambda)\mathcal{T}_\mathbf{l}^\dagger(0, t_0^{\lambda'})\right\rangle = \frac{1}{(2\pi a)^2} \times \prod_{j=1,2}\left(\frac{\pi a/(\beta_j v_j)}{\sin\left[\frac{\pi(a + i\chi_{\lambda,\lambda'}(t-t_0)(v_j(t-t_0)))}{v_j\beta_j}\right]}\right)^{2d_j}, \tag{C8}$$

where $\chi_{\lambda,\lambda'}(t - t_0) = \text{sgn}(t - t_0)(\lambda + \lambda')/2 - (\lambda - \lambda')/2$, $\beta_j = 1/T_j$ is the inverse temperature of channel j, and $d_j = l_j|\delta\nu_j|/2$ is the scaling dimension of $\exp(il_i\phi_i)$. The total scaling dimension is then $\Delta(\mathbf{l}) = \sum_j d_j$.

Inserting the Green's functions (C8) into Eq. (C7), we obtain

$$\begin{aligned}\langle I(t)\rangle &= \frac{q|\Gamma_0|^2}{(2\pi a)^2}\prod_k\left(\frac{\pi a}{v_k\beta_k}\right)^{2d_k}\sum_{\lambda,\lambda'=\pm1}\lambda'\\ &\times\int_{-\infty}^{\infty}dt_0\frac{\sin\left[\omega_0\left(t^{\lambda}-t_0^{\lambda'}\right)\right]}{\prod_j\sin\left[\frac{\pi}{v_j\beta_j}(a+i\chi_{\lambda,\lambda'}(t-t_0)v_j(t-t_0)\right]^{2d_j}}\\ &= \frac{q|\Gamma_0|^2}{(2\pi a)^2}\prod_k\left(\frac{\pi a}{v_k\beta_k}\right)^{2d_k}\sum_{\lambda=\pm1}\lambda\\ &\times\int_{-\infty}^{\infty}dt_0\frac{\sin[\omega_0(t-t_0)]}{\prod_j\sin\left[\frac{\pi}{v_j\beta_j}\left(a-i\lambda v_j(t-t_0)\right)\right]^{2d_j}}.\end{aligned}\tag{C9}$$

In the second equality, we used that when $\lambda=\lambda'$, the integrand becomes odd in $t-t_0$ and hence this contribution vanishes. We next assume that the two channels are at the same temperature: $T_j=T$ and also that $aT/v_j<1$ for $j=1$ and 2. We then change variables $t-t_0\to\lambda(t_0+i/(2T))$. To lowest order in b, the integral becomes

$$\begin{aligned}\langle I(t)\rangle &= \frac{q|\Gamma_0|^2}{(2\pi a)^2}\prod_k\left(\frac{\pi a}{v_k\beta_k}\right)^{2d_k}\sum_{\lambda=\pm1}\lambda\\ &\times\int_{-\infty}^{\infty}dt_0\frac{\sin[-\lambda\omega_0(t_0+i/(2T))]}{\prod_j\cosh(\pi Tt_0)^{2d_j}}\\ &= \frac{2q|\Gamma_0|^2}{(2\pi a)^2}\prod_k\left(\frac{\pi aT}{v_k}\right)^{2d_k}\sinh\left(\frac{\omega_0}{2T}\right)\\ &\times\int_{-\infty}^{\infty}dt_0\frac{\cos[\omega_0t_0]}{\prod_j\cosh(\pi Tt_0)^{2d_j}}\\ &= \frac{2q|\Gamma_0|^2}{(2\pi a)^2}(\pi aT)^{2\Delta(\mathbf{l})}\prod_k\left(\frac{1}{v_k}\right)^{2d_k}\sinh\left(\frac{\omega_0}{2T}\right)\\ &\times\int_{-\infty}^{\infty}dt_0\frac{\cos[\omega_0t_0]}{\cosh(\pi Tt_0)^{2\Delta(\mathbf{l})}}.\end{aligned}\tag{C10}$$

The final integral can now be performed with the identity $\int_{-\infty}^{\infty}dt\cosh(2yt)/\cosh^{2x}t=2^{2x-1}\Gamma(x+y)\Gamma(x-y)/\Gamma(2x)$, for $\mathrm{Re}\,x>|\mathrm{Re}\,y|$ and $\mathrm{Re}\,x>0$, with $\Gamma(z)$ the Gamma-function. We then find the time-independent tunneling current

$$\begin{aligned}\langle I\rangle\equiv\langle I(t)\rangle &= 2q|\Gamma_0|^2(2\pi a)^{2\Delta(\mathbf{l})-2}T^{2\Delta(\mathbf{l})-1}\\ &\times\prod_k\left(\frac{1}{v_k}\right)^{2d_k}\sinh\left(\frac{\omega_0}{2T}\right)\frac{\left|\Gamma\left(\Delta(\mathbf{l})+i\frac{\omega_0}{2\pi T}\right)\right|^2}{\Gamma(2\Delta(\mathbf{l}))},\end{aligned}\tag{C11}$$

as given in Eq. (95). In the high-temperature regime $\omega_0\ll T$, we find the Ohmic behavior

$$\langle I\rangle = g_\tau\frac{e^2}{h}(V_1-V_2),\tag{C12}$$

with the tunneling conductance

$$g_\tau\equiv q^2\frac{|\Gamma_0|^2(2\pi aT)^{2\Delta(\mathbf{l})-2}}{\prod_k v_k^{2d_k}}\frac{|\Gamma(\Delta(\mathbf{l}))|^2}{\Gamma(2\Delta(\mathbf{l}))},\tag{C13}$$

presented in Eq. (100) in the main text. We next consider the symmetrized noise

$$S(t,t')=\langle I(t)I(t')\rangle+\langle I(t')I(t)\rangle-2\langle I(t)\rangle\langle I(t')\rangle.\tag{C14}$$

To leading order in Γ_0, $S(t,t')$ is given on the Keldysh contour as

$$\begin{aligned}S(t,t')\equiv S(t-t') &= \sum_{\lambda=\pm1}\langle T_C[I(t^{\lambda})I(t'^{-\lambda})]\rangle\\ &= 2q^2|\Gamma_0|^2\sum_{\lambda=\pm1}\cos\left[\omega_0(t^{\lambda}-t_0^{\lambda'})\right]\\ &\times\left\langle T_C\mathcal{T}_{\mathbf{l}}(0,t^{\lambda})\mathcal{T}_{\mathbf{l}}^{\dagger}\left(0,t_0^{\lambda'}\right)\right\rangle.\end{aligned}\tag{C15}$$

We are interested in the zero frequency (dc) noise $S(\omega=0)\equiv\int d(t-t_0)S(t-t_0)$. The calculations proceed in perfect analogy to those for $\langle I\rangle$, and using Eq. (C11), we arrive at Eq. (96) in the main text, namely,

$$S(\omega=0)=2q\cosh\left(\frac{\omega_0}{2T}\right)\frac{\langle I\rangle}{\sinh\left(\frac{\omega_0}{2T}\right)}=2q\langle I\rangle\coth\left(\frac{\omega_0}{2T}\right).\tag{C16}$$

In the limit $\omega_0\ll T$, the noise approaches the equilibrium Nyquist-Johnson noise

$$S(\omega=0)=4g_\tau\frac{e^2}{h}k_BT.\tag{C17}$$

In the shot-noise limit $\omega_0\gg T$, the Fano factor F becomes

$$F\equiv\frac{S(\omega=0)}{2\langle I\rangle}=q\coth\left(\frac{\omega_0}{2T}\right)\xrightarrow[\omega_0\gg T]{}q,\tag{C18}$$

which is given in Eq. (99) in the main text. Eq. (C18) manifest the well-known result that weak tunneling reveals the charges of the transferred particles. Generalizations of this formula can be found in Refs. [64,65]. By use of Eqs. (92) and (93), the formula (C18) manifests how the tunneling charge is affected by generic charge vector entries t_1 and t_2. We emphasize again that F is independent of interactions in the free phase.

Since the tunneling operator $\mathcal{T}_{\mathbf{l}}$ so far has been treated as general, we must now determine the most relevant tunneling processes in the SBS and WBS regimes.

For point tunneling, the tree level RG equation for the tunneling amplitude Γ_0 can be read of directly from H_0+H_τ. The equation reads

$$\frac{\partial\Gamma_0}{\partial\ln(L/a)}=[1-\Delta(\mathbf{l})]\Gamma_0,\tag{C19}$$

where $\Delta(\mathbf{l})$ is the scaling dimension of $\mathcal{T}_{\mathbf{l}}$, L is the system size, and a is the UV length cutoff. The combination $\ln(L/a)$ parametrizes the RG flow. Under the assumption of no interchannel interactions across the constriction, the scaling dimension is obtained from the general scaling dimension formula (25) as

$$\Delta(\mathbf{l})=\tfrac{1}{2}(d_1+d_2)=\tfrac{1}{2}\left(|\delta\nu_1|l_1^2+|\delta\nu_2|l_2^2\right).\tag{C20}$$

This relation holds strictly only in the bound phase, where there is only a single channel propagating. In the free phase, with three edge channels, the scaling dimensions will be affected by interchannel interactions. However, since the free phase is characterized by weak interactions, we expect that the difference between Eq. (C20) and the true, "renormalized" scaling dimensions is small and can thus be ignored.

For the case of identical edge channels $|\delta\nu_1|=|\delta\nu_2|\equiv|\delta\nu|$, charge conservation requires $l_1 = l_2 \equiv l$. In this case, Eq. (C19) becomes

$$\frac{\partial\Gamma_0}{\partial\ln(L/a)} = (1 - l^2|\delta\nu|)\Gamma_0. \tag{C21}$$

Hence, the most relevant tunneling process is obtained for $l = 1$. Physically, this means that single-particle tunneling events dominate over multiparticle events. In the next sections, we apply Eqs. (C18), and (C21) to determine the most dominant Fano factors for the two edge phases Eqs. (40) and (45).

[1] D. C. Tsui, H. L. Stormer, and A. C. Gossard, Two-Dimensional Magnetotransport in the Extreme Quantum Limit, Phys. Rev. Lett. **48**, 1559 (1982).

[2] R. B. Laughlin, Anomalous Quantum Hall Effect: An Incompressible Quantum Fluid with Fractionally Charged Excitations, Phys. Rev. Lett. **50**, 1395 (1983).

[3] X. G. Wen, Topological orders in rigid states, Int. J. Mod. Phys. B **04**, 239 (1990).

[4] X. G. Wen, Chiral Luttinger liquid and the edge excitations in the fractional quantum Hall states, Phys. Rev. B **41**, 12838 (1990).

[5] X. G. Wen, Theory of the edge states in fractional quantum Hall effects, Int. J. Mod. Phys. B **06**, 1711 (1992).

[6] X.-G. Wen, Impurity effects on chiral one-dimensional electron systems, Phys. Rev. B **50**, 5420 (1994).

[7] X.-G. Wen, Topological orders and edge excitations in fractional quantum Hall states, Adv. Phys. **44**, 405 (1995).

[8] A. M. Chang, Chiral Luttinger liquids at the fractional quantum Hall edge, Rev. Mod. Phys. **75**, 1449 (2003).

[9] L. Saminadayar, D. C. Glattli, Y. Jin, and B. Etienne, Observation of the $e/3$ Fractionally Charged Laughlin Quasiparticle, Phys. Rev. Lett. **79**, 2526 (1997).

[10] R. de-Picciotto, M. Reznikov, M. Heiblum, V. Umansky, G. Bunin, and D. Mahalu, Direct observation of a fractional charge, Nature (London) **389**, 162 (1997).

[11] C. Lin, M. Hashisaka, T. Akiho, K. Muraki, and T. Fujisawa, Quantized charge fractionalization at quantum Hall y junctions in the disorder dominated regime, Nat. Commun. **12**, 131 (2021).

[12] J. Nakamura, S. Liang, G. C. Gardner, and M. J. Manfra, Direct observation of anyonic braiding statistics, Nat. Phys. **16**, 931 (2020).

[13] H. Bartolomei, M. Kumar, R. Bisognin, A. Marguerite, J.-M. Berroir, E. Bocquillon, B. Plaçais, A. Cavanna, Q. Dong, U. Gennser *et al.*, Fractional statistics in anyon collisions, Science **368**, 173 (2020).

[14] C. Nayak, S. H. Simon, A. Stern, M. Freedman, and S. Das Sarma, Non-Abelian anyons and topological quantum computation, Rev. Mod. Phys. **80**, 1083 (2008).

[15] C. L. Kane, M. P. A. Fisher, and J. Polchinski, Randomness at the Edge: Theory of Quantum Hall Transport at Filling $\nu = 2/3$, Phys. Rev. Lett. **72**, 4129 (1994).

[16] C. L. Kane and M. P. A. Fisher, Impurity scattering and transport of fractional quantum Hall edge states, Phys. Rev. B **51**, 13449 (1995).

[17] J. E. Moore and X.-G. Wen, Classification of disordered phases of quantum Hall edge states, Phys. Rev. B **57**, 10138 (1998).

[18] H.-c. Kao, C.-H. Chang, and X.-G. Wen, Binding Transition in Quantum Hall Edge States, Phys. Rev. Lett. **83**, 5563 (1999).

[19] F. D. M. Haldane, Stability of Chiral Luttinger Liquids and Abelian Quantum Hall States, Phys. Rev. Lett. **74**, 2090 (1995).

[20] M. Heiblum and D. E. Feldman, Edge probes of topological order, Int. J. Mod. Phys. A **35**, 2030009 (2020).

[21] M. Banerjee, M. Heiblum, A. Rosenblatt, Y. Oreg, D. E. Feldman, A. Stern, and V. Umansky, Observed quantization of anyonic heat flow, Nature (London) **545**, 75 (2017).

[22] M. Banerjee, M. Heiblum, V. Umansky, D. E. Feldman, Y. Oreg, and A. Stern, Observation of half-integer thermal Hall conductance, Nature (London) **559**, 205 (2018).

[23] S. K. Srivastav, M. R. Sahu, K. Watanabe, T. Taniguchi, S. Banerjee, and A. Das, Universal quantized thermal conductance in graphene, Sci. Adv. **5**, eaaw5798(2019).

[24] S. K. Srivastav, R. Kumar, C. Spånslätt, K. Watanabe, T. Taniguchi, A. D. Mirlin, Y. Gefen, and A. Das, Vanishing Thermal Equilibration for Hole-Conjugate Fractional Quantum Hall States in Graphene, Phys. Rev. Lett. **126**, 216803 (2021).

[25] R. A. Melcer, B. Dutta, C. Spånslätt, J. Park, A. D. Mirlin, and V. Umansky, Absent thermal equilibration on fractional quantum Hall edges over macroscopic scale, Nat. Commun. **13**, 376 (2022).

[26] R. Kumar, S. K. Srivastav, C. Spånslätt, K. Watanabe, T. Taniguchi, Y. Gefen, A. D. Mirlin, and A. Das, Observation of ballistic upstream modes at fractional quantum Hall edges of graphene, Nat. Commun. **13**, 213 (2022).

[27] S. K. Srivastav, R. Kumar, C. Spånslätt, K. Watanabe, T. Taniguchi, A. D. Mirlin, Y. Gefen, and A. Das, Determination of topological edge quantum numbers of fractional quantum Hall phases by thermal conductance measurements, Nat. Commun. **13**, 5185 (2022).

[28] G. Le Breton, R. Delagrange, Y. Hong, M. Garg, K. Watanabe, T. Taniguchi, R. Ribeiro-Palau, P. Roulleau, P. Roche, and F. D. Parmentier, Heat Equilibration of Integer and Fractional Quantum Hall Edge Modes in Graphene, Phys. Rev. Lett. **129**, 116803 (2022).

[29] Y. Cohen, Y. Ronen, W. Yang, D. Banitt, J. Park, M. Heiblum, A. D. Mirlin, Y. Gefen, and V. Umansky, Synthesizing a $\nu = 2/3$ fractional quantum Hall effect edge state from counter-propagating $\nu = 1$ and $\nu = 1/3$ states, Nat. Commun. **10**, 1920 (2019).

[30] F. Lafont, A. Rosenblatt, M. Heiblum, and V. Umansky, Counter-propagating charge transport in the quantum Hall effect regime, Science **363**, 54 (2019).

[31] B. Dutta, V. Umansky, M. Banerjee, and M. Heiblum, Isolated ballistic non-Abelian interface channel, Science **377**, 1198 (2022).

[32] B. Dutta, W. Yang, R. Melcer, H. K. Kundu, M. Heiblum, V. Umansky, Y. Oreg, A. Stern, and D. Mross, Distinguishing between non-Abelian topological orders in a quantum Hall system, Science **375**, 193 (2022).

[33] C. L. Kane and M. P. A. Fisher, Quantized thermal transport in the fractional quantum Hall effect, Phys. Rev. B **55**, 15832 (1997).

[34] A. Cappelli, M. Huerta, and G. R. Zemba, Thermal transport in chiral conformal theories and hierarchical quantum Hall states, Nucl. Phys. B **636**, 568 (2002).

[35] T. Giamarchi and H. J. Schulz, Anderson localization and interactions in one-dimensional metals, Phys. Rev. B **37**, 325 (1988).

[36] I. V. Gornyi, A. D. Mirlin, and D. G. Polyakov, Electron transport in a disordered Luttinger liquid, Phys. Rev. B **75**, 085421 (2007).

[37] C. Murthy and C. Nayak, Almost Perfect Metals in One Dimension, Phys. Rev. Lett. **124**, 136801 (2020).

[38] I. Protopopov, Y. Gefen, and A. Mirlin, Transport in a disordered $\nu = 2/3$ fractional quantum Hall junction, Ann. Phys. **385**, 287 (2017).

[39] C. Spånslätt, J. Park, Y. Gefen, and A. D. Mirlin, Topological Classification of Shot Noise on Fractional Quantum Hall Edges, Phys. Rev. Lett. **123**, 137701 (2019).

[40] H. Asasi and M. Mulligan, Partial equilibration of anti-Pfaffian edge modes at $\nu = 5/2$, Phys. Rev. B **102**, 205104 (2020).

[41] C. L. Kane and M. P. A. Fisher, Contacts and edge-state equilibration in the fractional quantum Hall effect, Phys. Rev. B **52**, 17393 (1995).

[42] C. Nosiglia, J. Park, B. Rosenow, and Y. Gefen, Incoherent transport on the $\nu = 2/3$ quantum Hall edge, Phys. Rev. B **98**, 115408 (2018).

[43] J. Park, A. D. Mirlin, B. Rosenow, and Y. Gefen, Noise on complex quantum Hall edges: Chiral anomaly and heat diffusion, Phys. Rev. B **99**, 161302(R) (2019).

[44] Christian Spånslätt, J. Park, Y. Gefen, and A. D. Mirlin, Conductance plateaus and shot noise in fractional quantum Hall point contacts, Phys. Rev. B **101**, 075308 (2020).

[45] J. Park, C. Spånslätt, Y. Gefen, and A. D. Mirlin, Noise on the Non-Abelian $\nu = 5/2$ Fractional Quantum Hall Edge, Phys. Rev. Lett. **125**, 157702 (2020).

[46] M. Hein and C. Spånslätt, Thermal conductance and noise of Majorana modes along interfaced $\nu = 5/2$ fractional quantum Hall states, arXiv:2211.08000 [Phys. Rev. B (to be published)].

[47] L. Fidkowski, X. Chen, and A. Vishwanath, Non-Abelian Topological Order on the Surface of a 3D Topological Superconductor from an Exactly Solved Model, Phys. Rev. X **3**, 041016 (2013).

[48] D. T. Son, Is the Composite Fermion a Dirac Particle? Phys. Rev. X **5**, 031027 (2015).

[49] P. T. Zucker and D. E. Feldman, Stabilization of the Particle-Hole Pfaffian Order by Landau-Level Mixing and Impurities That Break Particle-Hole Symmetry, Phys. Rev. Lett. **117**, 096802 (2016).

[50] L. Antonić, J. Vučičević, and M. V. Milovanović, Paired states at 5/2: Particle-hole Pfaffian and particle-hole symmetry breaking, Phys. Rev. B **98**, 115107 (2018).

[51] R. Willett, J. P. Eisenstein, H. L. Störmer, D. C. Tsui, A. C. Gossard, and J. H. English, Observation of an Even-Denominator Quantum Number in the Fractional Quantum Hall Effect, Phys. Rev. Lett. **59**, 1776 (1987).

[52] G. Moore and N. Read, Nonabelions in the fractional quantum Hall effect, Nucl. Phys. B **360**, 362 (1991).

[53] C. Spånslätt, Y. Gefen, I. V. Gornyi, and D. G. Polyakov, Contacts, equilibration, and interactions in fractional quantum Hall edge transport, Phys. Rev. B **104**, 115416 (2021).

[54] S. Jézouin, F. D. Parmentier, A. Anthore, U. Gennser, A. Cavanna, Y. Jin, and F. Pierre, Quantum limit of heat flow across a single electronic channel, Science **342**, 601 (2013).

[55] I. V. Krive, Thermal transport through Luttinger liquid constriction, Low Temp. Phys. **24**, 377 (1998).

[56] I. Safi and H. J. Schulz, Transport in an inhomogeneous interacting one-dimensional system, Phys. Rev. B **52**, R17040 (1995).

[57] C. L. Kane and M. P. A. Fisher, Nonequilibrium Noise and Fractional Charge in the Quantum Hall Effect, Phys. Rev. Lett. **72**, 724 (1994).

[58] C. d. C. Chamon, D. E. Freed, and X. G. Wen, Tunneling and quantum noise in one-dimensional Luttinger liquids, Phys. Rev. B **51**, 2363 (1995).

[59] P. Fendley, A. W. W. Ludwig, and H. Saleur, Exact Nonequilibrium dc Shot Noise in Luttinger Liquids and Fractional Quantum Hall Devices, Phys. Rev. Lett. **75**, 2196 (1995).

[60] D. E. Feldman and M. Heiblum, Why a noninteracting model works for shot noise in fractional charge experiments, Phys. Rev. B **95**, 115308 (2017).

[61] T. Martin, Noise in mesoscopic physics, in *Proceedings of the Les Houches Summer School, Session LXXXI*, edited by H. Bouchiat, Y. Gefen, S. Guéron, G. Montambaux, and J. Dalibard (Elsevier, New York, 2005).

[62] S. Biswas, R. Bhattacharyya, H. K. Kundu, A. Das, M. Heiblum, V. Umansky, M. Goldstein, and Y. Gefen, Shot noise does not always provide the quasiparticle charge, Nat. Phys. **18**, 1476 (2022).

[63] B. Overbosch and X.-G. Wen, Phase transitions on the edge of the $\nu = 5/2$ Pfaffian and anti-Pfaffian quantum Hall state, arXiv:0804.2087.

[64] F. Dolcini, B. Trauzettel, I. Safi, and H. Grabert, Transport properties of single-channel quantum wires with an impurity: Influence of finite length and temperature on average current and noise, Phys. Rev. B **71**, 165309 (2005).

[65] B. Roussel, P. Degiovanni, and I. Safi, Perturbative fluctuation dissipation relation for nonequilibrium finite-frequency noise in quantum circuits, Phys. Rev. B **93**, 045102 (2016).